



# Calsyntenin-3 interacts with both $\alpha$ - and $\beta$ -neurexins in the regulation of excitatory synaptic innervation in specific Schaffer collateral pathways

Received for publication, February 17, 2020, and in revised form, May 15, 2020. Published, Papers in Press, May 19, 2020, DOI 10.1074/jbc.RA120.013077

Hyeonho Kim<sup>1</sup>, Dongwook Kim<sup>1</sup>, Jinhu Kim<sup>1</sup>, Hee-Yoon Lee<sup>2</sup>, Dongseok Park<sup>1</sup>, Hyeeyeon Kang<sup>1</sup>, Keiko Matsuda<sup>3</sup>, Fredrik H. Sterky<sup>4,5</sup>, Michisuke Yuzaki<sup>3</sup>, Jin Young Kim<sup>6</sup>, Se-Young Choi<sup>2</sup>, Jaewon Ko<sup>1,\*</sup>, and Ji Won Um<sup>1,7,\*</sup>

From the <sup>1</sup>Department of Brain and Cognitive Sciences, Daegu Gyeongbuk Institute of Science and Technology (DGIST), Hyeonpoong-Eup, Dalseong-gun, Daegu, Korea, the <sup>2</sup>Department of Neuroscience and Physiology, Dental Research Institute, School of Dentistry, Seoul National University, Seoul, Korea, the <sup>3</sup>Department of Physiology, School of Medicine, Keio University, Tokyo, Japan, the <sup>4</sup>Wallenberg Centre for Molecular and Translational Medicine, <sup>5</sup>Department of Laboratory Medicine, University of Gothenburg, Gothenburg, Sweden, the <sup>6</sup>Biomedical Omics Group, Korea Basic Science Institute, Cheongju, Chungbuk, Korea, and the <sup>7</sup>Core Protein Resources Center, Daegu Gyeongbuk Institute of Science and Technology (DGIST), Hyeonpoong-Eup, Dalseong-Gun, Daegu, Korea

Edited by Paul E. Fraser

Calsyntenin-3 (Clstn3) is a postsynaptic adhesion molecule that induces presynaptic differentiation via presynaptic neurexins (Nrxns), but whether Nrxns directly bind to Clstn3 has been a matter of debate. Here, using LC–MS/MS–based protein analysis, confocal microscopy, RNAscope assays, and electrophysiological recordings, we show that  $\beta$ -Nrxns directly interact via their LNS domain with Clstn3 and Clstn3 cadherin domains. Expression of splice site 4 (SS4) insert–positive  $\beta$ -Nrxn variants, but not insert–negative variants, reversed the impaired Clstn3 synaptogenic activity observed in Nrxn-deficient neurons. Consistently, Clstn3 selectively formed complexes with SS4–positive Nrxns *in vivo*. Neuron-specific Clstn3 deletion caused significant reductions in number of excitatory synaptic inputs. Moreover, expression of Clstn3 cadherin domains in CA1 neurons of Clstn3 conditional knockout mice rescued structural deficits in excitatory synapses, especially within the stratum radiatum layer. Collectively, our results suggest that Clstn3 links to SS4–positive Nrxns to induce presynaptic differentiation and orchestrate excitatory synapse development in specific hippocampal neural circuits, including Schaffer collateral afferents.

Synaptogenic adhesion molecules, a class of synaptic transmembrane proteins that induce synaptic differentiation *in vitro* (1–3), are central to various aspects of synapse development, but their precise roles in synapse assembly, validation, and/or plasticity *in vivo* are only beginning to be revealed (1, 4, 5). Presynaptic neurexins (Nrxns) and leukocyte common antigen-related receptor protein-tyrosine phosphatases (LAR-RPTPs) are among the synaptogenic adhesion molecules that have emerged as key platforms that facilitate convergence of diverse signals from multifarious postsynaptic ligands at mammalian synapses (5, 6). Of particular note is the fact that, although Nrxns and LAR-RPTPs are evolutionarily conserved, only a

subset of their ligands in mammals has homologs in invertebrate species that also play crucial roles in various aspects of central nervous system development, hinting at the possibility that Nrxns and LAR-RPTPs serve fundamental functions through these selective adhesion pathways.

Calsyntenins (Clstns) are evolutionarily conserved synaptogenic adhesion proteins of the cadherin superfamily that are expressed most highly in the brain (7). Synaptic functions of the three vertebrate Clstn family members have recently been reported. For example, juvenile Clstn1-deficient mice exhibit compromised excitatory synaptic transmission, possibly because of disrupted targeting of *N*-methyl-D-aspartate (NMDA) receptor subunits (8). They also show increased synaptic levels of GluN2B subunit-containing NMDA receptors, enhanced long-term potentiation (LTP), and greater filopodia-like dendritic protrusions in the hippocampus, but decreased dendritic arborization, suggesting that Clstn1 mediates dendritic transport of NMDA receptor subunits and regulates spine maturation during early development (8). In addition, Clstn1 regulates guidance receptor trafficking by shuttling Rab11-positive vesicles, leading to switching of commissural axon responsiveness (9). Clstn1 also contributes to peripheral sensory axon arborization, branching, endosomal dynamics, and microtubule polarity in zebrafish (10, 11). Clstn2, on the other hand, plays a nonredundant role in inhibitory synapse development and influences a subset of cognitive abilities (12, 13). Clstn3 was identified as a postsynaptic adhesion molecule that acts through presynaptic Nrxns (14, 15). However, in contrast to the report of Pettem *et al.* (14), we did not detect direct interactions between Clstn3 and  $\alpha$ -Nrxns.

In the present study, we revisited these issues. Strikingly, utilizing newly engineered Nrxn1 expression vectors to increase Nrxn1 $\beta$  expression levels, we found that recombinant Clstn3 bound both Nrxn1 $\beta$  and Nrxn1 $\alpha$ , with a slight preference for splice site 4 (SS4) insert–positive variants, requiring an Nrxn splice variant containing an insert at SS4 as a functional receptor for its presynaptic differentiation-inducing activity. Conditional

This article contains supporting information.

\*For correspondence: Jaewon Ko, [jaewonko@dgist.ac.kr](mailto:jaewonko@dgist.ac.kr); Ji Won Um, [jwum@dgist.ac.kr](mailto:jwum@dgist.ac.kr).

deletion of *Clstn3* in neurons led to drastic reductions in excitatory synapse structures. Finally, adeno-associated virus-mediated expression of Nrxn-binding CST-3 cadherin domains was sufficient to rescue decreased excitatory synapse puncta density in CA1 stratum radiatum layers of *Clstn3*-deficient mice. Viewed together, our results revise our previous molecular model, showing that *Clstn3* directly interacts with SS4-positive Nrxn splice variants to induce presynaptic differentiation, and suggesting synapse-organizing functions of *Clstn3* that may control specific synaptic inputs from Schaffer-collateral afferents in the hippocampus.

## Results

### *Clstn3* directly binds $\beta$ -Nrxns

Our previous cell surface-binding assays used a variety of Nrxn1 $\alpha$  deletion variants derived from the bovine *Nrxn1 $\alpha$*  gene or Nrxn1 $\beta$  variants derived from the rat *Nrxn1 $\beta$*  gene (15). These vectors have long been used to characterize Nrxn interactions with neuroligins (NLs) and other ligands, including leucine-rich repeat transmembrane neuronal proteins (LRRTMs), neurexophilins, and latrophilin-1 (16–18). However, using Nrxn vectors constructed from mouse *Nrxn* genes, Craig and colleagues (14) reported that Nrxn1 $\alpha$ , but not Nrxn1 $\beta$ , binds to *Clstn3*. To resolve this discrepancy, we performed affinity chromatography of solubilized mouse synaptosomes using immobilized recombinant IgClstn3 followed by MS. Intriguingly, among the captured proteins was a tryptic peptide unique to Nrxn1 $\beta$  (in addition to Nrxn1 $\alpha$  peptides) (Fig. 1, A–D; Table S1). To confirm binding between *Clstn3* and Nrxn1 $\beta$ , we engineered mouse Nrxn1 $\beta$  expression constructs and performed cell surface-binding assays. We found robust binding of IgClstn3 to HEK293T cells expressing C terminally FLAG-tagged mNrxn1 $\beta$  lacking (mNrxn1 $\beta$ <sup>-SS4</sup>-FLAG) or containing (mNrxn1 $\beta$ <sup>+SS4</sup>-FLAG) the SS4 insert (Fig. 1, E and F). In assays measuring dimeric ligand binding to mNrxn-expressing cell surfaces, IgClstn3 interacted with both mNrxn1 $\beta$ <sup>-SS4</sup> and mNrxn1 $\beta$ <sup>+SS4</sup> with nanomolar affinity (Fig. 1, G and H).  $K_d$  values calculated by Scatchard analyses were  $51.39 \pm 5.26$  nM for Nrxn1 $\beta$ <sup>+SS4</sup> and  $105.94 \pm 7.89$  nM for Nrxn1 $\beta$ <sup>-SS4</sup> (Fig. 1, G and H). These findings indicate that *Clstn3* binds Nrxn1 $\beta$  with high affinity and exhibits a slight preference for SS4 insert-positive splice variants. To investigate differences between bovine and rat Nrxn1 plasmids (bNrxn1 $\alpha$  and rNrxn1 $\beta$ ) used in our previous studies and the mouse Nrxn1 plasmids (mNrxn1 $\alpha$  and mNrxn1 $\beta$ ) used in the current study, we compared total protein expression levels produced by the different vectors by immunoblot analysis using serially diluted lysates from HEK293T cells transfected with expression plasmids for mNrxn and bNrxn1 $\alpha$  or rNrxn1 $\beta$  (Fig. S1). Surprisingly, expression levels of mNrxn vectors were ~100-fold higher than those of bNrxn and rNrxn vectors (Fig. S1A). This difference in expression was not likely attributable to differences in the position of the FLAG epitope between rNrxn1 $\beta$  (N terminus) and our original mNrxn1 $\beta$  construct, as evidenced by the comparably robust binding of a newly generated N terminally FLAG-tagged mNrxn1 $\beta$ <sup>+SS4</sup> (FLAG-mNrxn1 $\beta$ <sup>+SS4</sup>) and our original C terminally FLAG-

tagged mNrxn1 $\beta$ <sup>+SS4</sup> (mNrxn1 $\beta$ <sup>+SS4</sup>-FLAG) to IgClstn3 in cell surface-binding assays (Fig. S1, B and C).

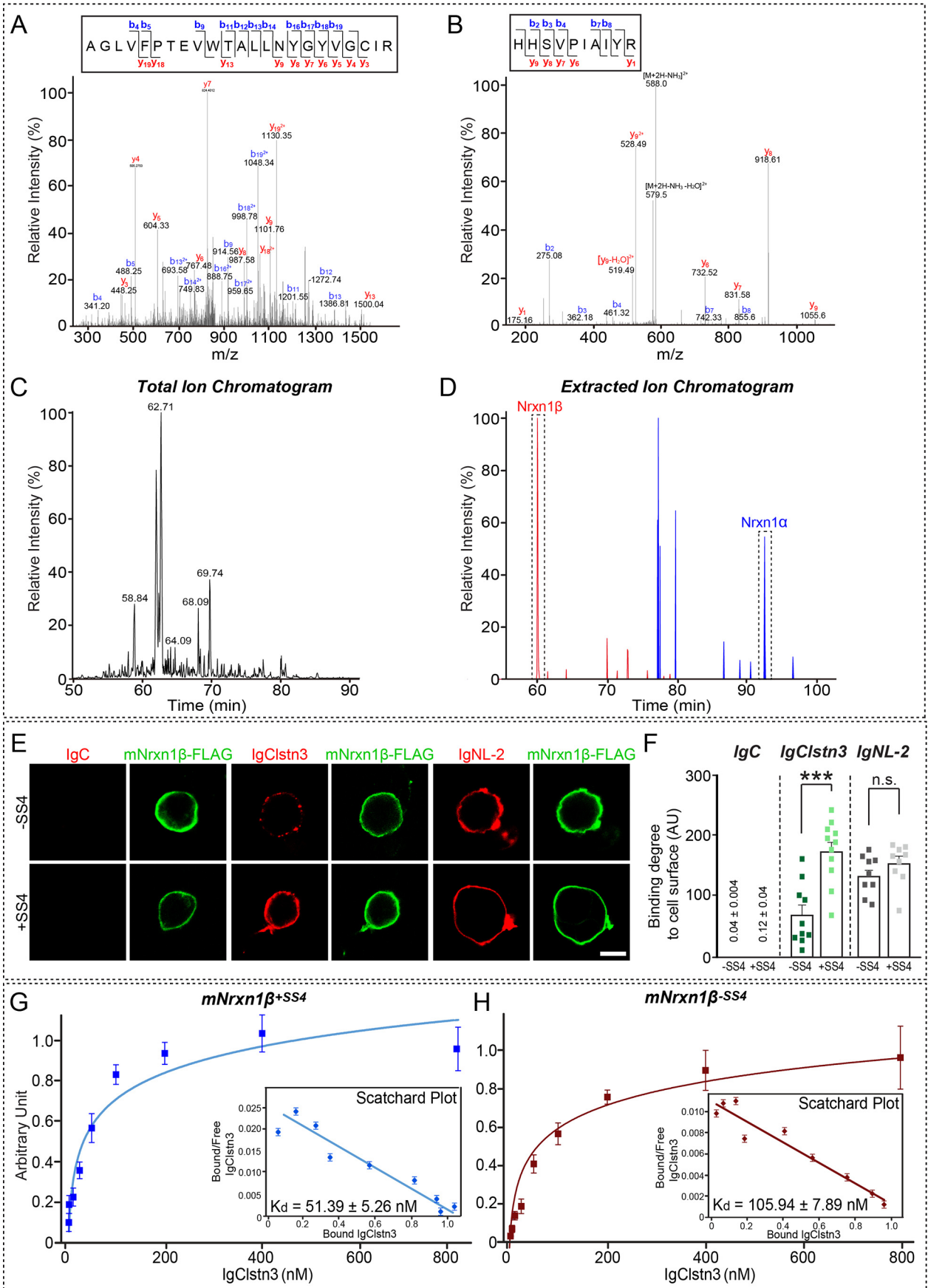
### Cadherin domains of *Clstn3* mediate direct binding to $\beta$ -Nrxns

In addition to cell surface-binding assays, *in vitro* pulldown assays clearly showed binding of *Clstn3* to IgmNrxn1 $\beta$ <sup>+SS4</sup> and IgmNrxn1 $\alpha$ <sup>+SS4</sup>. To identify a minimal *Clstn3* domain involved in Nrxn binding, we used three different FLAG-tagged *Clstn3* constructs: Full (full-length *Clstn3*), Cad (containing tandem cadherin domains, the transmembrane segment and intracellular residues of *Clstn3*), and  $\Delta$ Cad (full-length *Clstn3* lacking the tandem cadherin domains) (see Fig. 2A for schematic diagram of *Clstn3* constructs). IgmNrxn1 $\alpha$ <sup>+SS4</sup> and IgmNrxn1 $\beta$ <sup>+SS4</sup> both pulled down *Clstn3* Cad, but not *Clstn3*  $\Delta$ Cad (Fig. 2, B and C), suggesting that cadherin domains of *Clstn3* mediate binding to Nrxns. The results of these and aforementioned cell-based surface-binding assays do not exclude the possibility that intermediate(s) expressed in HEK293T cells may bridge indirect associations of Nrxns with *Clstn3*. However, binding assays performed using purified recombinant IgNrxn1 (IgNrxn1 $\beta$ <sup>-SS4</sup>, IgNrxn1 $\beta$ <sup>+SS4</sup>, IgNrxn1 $\alpha$ <sup>-SS4</sup>, or IgNrxn1 $\alpha$ <sup>+SS4</sup>) and recombinant His-HA-*Clstn3* (*Clstn3* Ecto, *Clstn3* Cad, or *Clstn3*  $\Delta$ Cad) (Fig. 2D) showed that His-HA-*Clstn3* Ecto directly bound to recombinant  $\alpha$ - and  $\beta$ -Nrxns (Fig. 2, E and F). Moreover, *Clstn3* Cad, but not *Clstn3*  $\Delta$ Cad, directly bound to recombinant  $\beta$ -Nrxns (Fig. 2F). These data suggest that cadherin domains of *Clstn3* mediate direct interactions with Nrxns, consistent with our previous observation that the cadherin domains of *Clstn3* are necessary and sufficient to induce presynaptic differentiation (15).

### *Clstn3* binds to an LNS domain of mNrxn1 $\beta$ in a $Ca^{2+}$ -dependent manner

We next investigated which Nrxn sequences mediate *Clstn3* binding. To this end, we generated the following FLAG-tagged mNrxn1 $\beta$ -deletion constructs: mNrxn1 $\beta$   $\Delta$ HRD, which lacks a  $\beta$ -Nrxn-unique histidine-rich sequence; mNrxn1 $\beta$   $\Delta$ LNS, which lacks a  $\beta$ -Nrxn LNS domain; and  $\Delta$ Stalk1, which lacks the entire stalk region (Fig. 3A). We found that IgClstn3 bound comparably to HEK293T cells expressing mNrxn1 $\beta$   $\Delta$ HRD or mNrxn1 $\beta$  WT, but did not bind HEK293T cells expressing mNrxn1 $\beta$   $\Delta$ LNS (Fig. 3, B and C), indicating that the Nrxn1 $\beta$  LNS domain is necessary for *Clstn3* binding. Interestingly, deletion of the entire stalk region (mNrxn1 $\beta$   $\Delta$ Stalk1) diminished *Clstn3* binding as well as NL-2 binding (Fig. 3, B and C). The stalk region contains ~40 residues with several putative O-linked glycosylated sites and a short cysteine-loop sequence composed of two conserved cysteines flanking an 8-residue acidic sequence (19). We thus hypothesized that O-linked glycosylation of mNrxn $\beta$  regulates *Clstn3* binding and that mNrxn1 $\beta$   $\Delta$ Stalk1 displayed weak *Clstn3* binding because it lacks O-linked glycosylation. To test this, we generated mNrxn1 $\beta$  constructs containing point mutations or deletions in the conserved stalk region. *Clstn3* binding was retained in mNrxn1 $\beta$  constructs in which putative O-glycosylated threonines

Interaction of *Clstn3* with  $\alpha/\beta$ -Nrxns



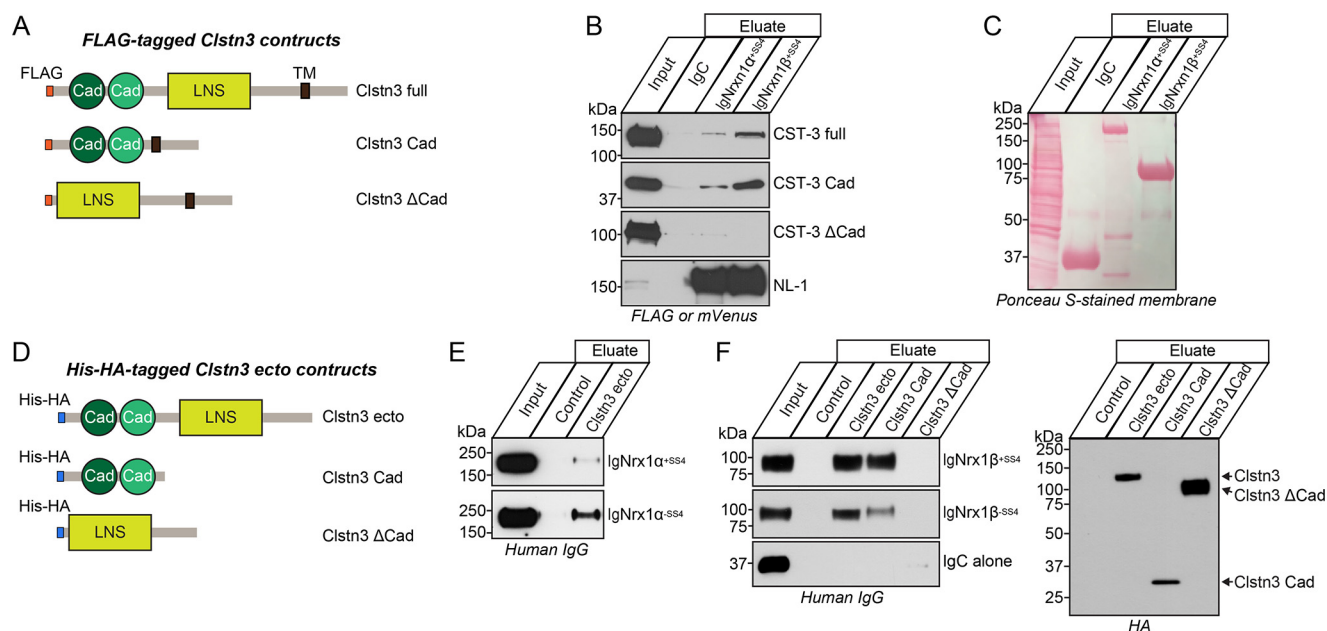


**Figure 2. Direct binding of Clstn3 cadherin domains to  $\beta$ -Nrxns.** *A*, diagrams of Clstn3 variants used in pull-down assays presented in *B*. *B*, IgNrxn1 $\alpha$ <sup>+SS4</sup>, IgNrxn1 $\beta$ <sup>+SS4</sup>, or IgC (negative control) proteins pulled down FLAG-Clstn3 Full and FLAG-Clstn3 Cad, but not FLAG-Clstn3  $\Delta$ Cad. *Input*, 5%. *C*, IgNrxn1 $\alpha$ <sup>+SS4</sup>, IgNrxn1 $\beta$ <sup>+SS4</sup>, or IgC used for pull-down assays were analyzed by direct comparison of bands revealed by parallel Ponceau S staining. *D*, diagrams of His-HA-tagged extracellular Clstn3 variants used in direct-binding assays. *E* and *F*, purified His-tagged Clstn3 proteins were incubated with purified IgNrxn proteins, as indicated. Precipitates obtained using Talon resin were analyzed by immunoblotting with human IgG or HA antibodies. *Input*, 10%.

or serines were replaced with glycines (mNrxn1 $\beta$   $\Delta$ CHO), the cysteine-loop sequence was deleted (mNrxn1 $\beta$   $\Delta$ CysL), the stalk region was partially deleted (mNrxn1 $\beta$   $\Delta$ Stalk2), or the conserved serine residue for attaching heparan sulfate chains was replaced with alanine (mNrxn1 $\beta$   $\Delta$ HS) (Fig. 4, *A–D* and *F*). However, Clstn3 did not bind Nrxn1 $\gamma$ , a newly identified Nrxn1 isoform (19), or other heparan sulfate proteoglycans, such as glypicans or syndecans (Figs. 3, *B* and *C*, and 4, *E* and *F*). Control experiments showed that surface expression levels of individual mNrxn1 $\beta$  deletion constructs in HEK293T cells were comparable with those of WT protein (Fig. S2). These findings suggest that the Nrxn1 $\beta$  LNS domain is a Clstn3-binding site. We further found that treatment with the Ca<sup>2+</sup> chelator EGTA prevented these interactions (Fig. S3).

### Clstn3 requires specific Nrxn splice variants for presynaptic differentiation

To delineate the molecular mechanisms that link Nrxns to Clstn3 and support its synaptogenic activity, we performed heterologous synapse-formation assays in cultured hippocampal neu-

rons in which all three Nrxns were down-regulated using small hairpin RNAs (15, 20). We found that Nrxns triple-knockdown (TKD) significantly reduced the synaptogenic activity of Clstn3 (Fig. 5, *A* and *B*) (15). Synaptogenic activity was completely restored by coexpression of Nrxn1 $\alpha$ <sup>+SS4</sup> or Nrxn1 $\beta$ <sup>+SS4</sup>, but not Nrxn1 $\alpha$ <sup>-SS4</sup> or Nrxn1 $\beta$ <sup>-SS4</sup>, suggesting that SS4-positive Nrxns act as functional receptors for Clstn3 (Fig. 5, *A* and *5B*, Fig. S4, *A* and *B*). Moreover, other SS4-positive  $\beta$ -Nrxns (Nrxn2 $\beta$ <sup>+SS4</sup> and Nrxn3 $\beta$ <sup>+SS4</sup>) also rescued the lost synaptogenic activity in Nrxn-TKD neurons (Fig. S4, *C* and *D*). Similarly, re-expression of the respective Nrx splice variants rescued deficits in the synaptogenic activities of NL-1 (neuroligin-1) and LRRTM2 (leucine-rich repeat transmembrane neuronal 2) (Fig. 5, *A* and *B*). Subsequent pull-down assays showed that IgNrxn1 $\alpha$ <sup>+SS4</sup> and IgNrxn1 $\beta$ <sup>+SS4</sup>, but not IgNrxn1 $\alpha$ <sup>-SS4</sup> or IgNrxn1 $\beta$ <sup>-SS4</sup>, were capable of capturing Clstn3 from mouse synaptosomal membrane fractions (Fig. 5, *C* and *D*). Moreover, re-expression of Nrxn1 $\beta$ <sup>+SS4</sup> in Nrxn-TKD neurons triggered clustering of both the inhibitory presynaptic marker GAD67 (glutamic acid decarboxylase 67) and the excitatory presynaptic marker VGLUT1 (vesicular glutamate transporter

**Figure 1. Analysis of Clstn3– $\beta$ -Nrxn interactions by MS and cell surface-binding assays.** *A* and *B*, MS/MS spectra of two double-charged peptides unique to Nrxn1 $\alpha$  and Nrxn1 $\beta$  at *m/z* 867.11 and 596.33, respectively, were obtained by liquid chromatography (LC)-MS/MS and fragmented to produce MS/MS spectra with *b*- and *y*-ion series describing the sequences AGLVFPTEVWTALLNYGYVGCIR (aa 501–523) and HHSVPIAIYR (aa 64–73). *C* and *D*, MS data. *C*, total ion chromatogram (XIC) of tryptic digests of Ig-Clstn3-bound eluates separated by LC. *D*, extracted ion chromatograms of *m/z* 867.11 and 596.33 ions from Nrxn1 $\alpha$  (92.8 min) and Nrxn1 $\beta$  (60.1 min), respectively. *E*, cell surface-binding assays. HEK293T cells expressing C terminally FLAG-tagged mouse Nrxns were incubated with purified Ig-fused neuroligin-2 (IgNL-2), calstentenin-3 (IgClstn3), or negative control (IgC) and analyzed by immunofluorescence imaging for Ig-fusion proteins (red) and FLAG (green). All binding reactions were performed in 2 mM CaCl<sub>2</sub> and 2 mM MgCl<sub>2</sub>. Scale bars: 10  $\mu$ m (applies to all images). *F*, quantification of cell surface binding in *E*. Data are mean  $\pm$  S.E. (\*\*\*, *p* < 0.001; nonparametric Mann-Whitney U test; number of cells analyzed = 9–11). *p* value for IgC binding: Nrxn1 $\beta$ <sup>-SS4</sup> versus Nrxn1 $\beta$ <sup>+SS4</sup>, *p* = 0.0630, *p* value for IgC binding: Nrxn1 $\beta$ <sup>-SS4</sup> versus Nrxn1 $\beta$ <sup>+SS4</sup>, *p* = 0.0003. *p* value for IgClstn3 binding: Nrxn1 $\beta$ <sup>-SS4</sup> versus Nrxn1 $\beta$ <sup>+SS4</sup>, *p* = 0.1903. *p* value for IgNL-2 binding: Nrxn1 $\beta$ <sup>-SS4</sup> versus Nrxn1 $\beta$ <sup>+SS4</sup>, *p* = 0.0630. *G* and *H*, saturation binding of IgClstn3 to FLAG-tagged mouse Nrxn1 $\beta$ <sup>+SS4</sup> (*G*) or Nrxn1 $\beta$ <sup>-SS4</sup> (*H*) expressed in HEK293T cells. *Inset*: Scatchard plot generated by linear regression of the data; *K<sub>d</sub>* was calculated from three independent experiments. Data are mean  $\pm$  S.E.

## Interaction of *Clstn3* with $\alpha/\beta$ -Nrxns

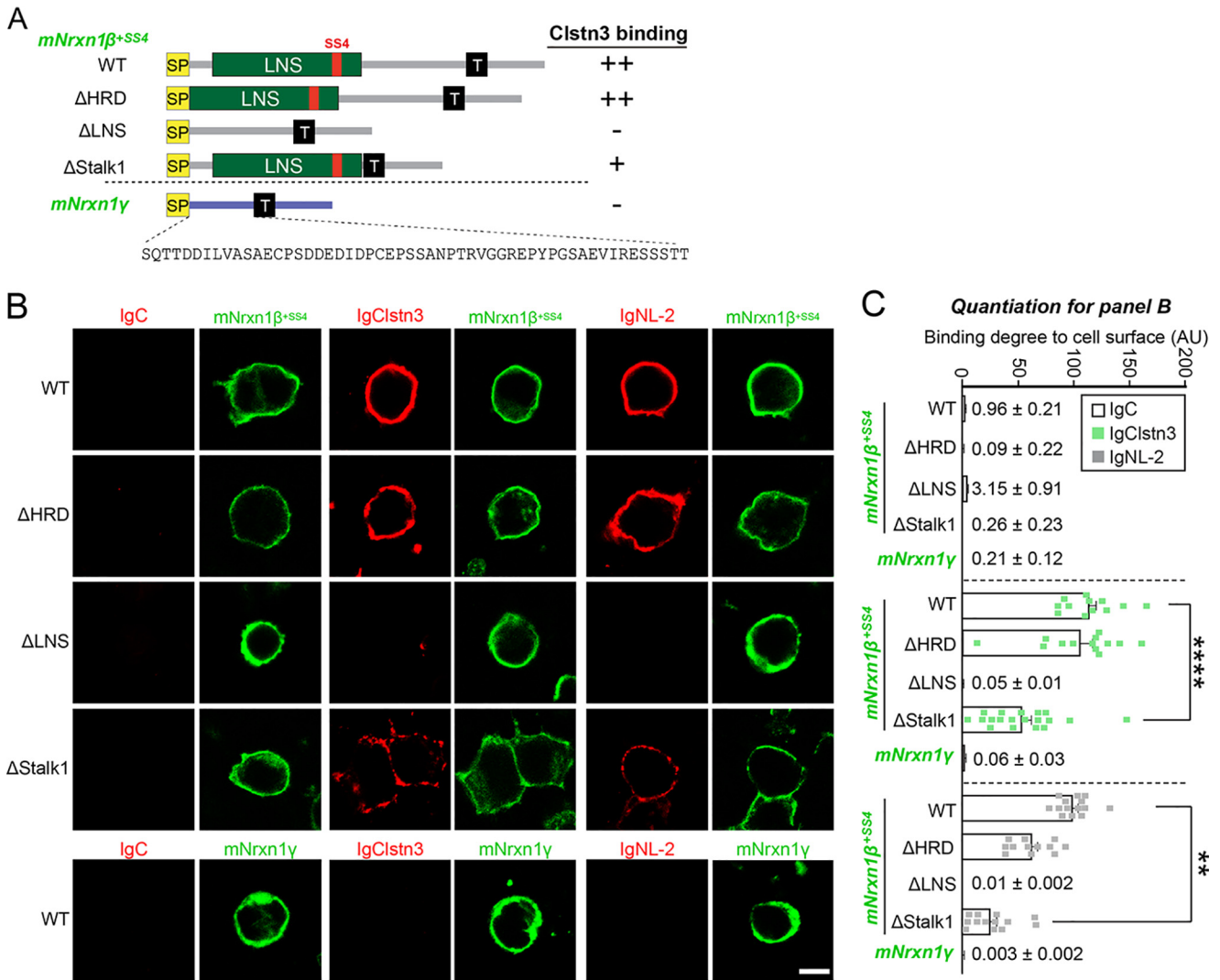


**Figure 3.** *Clstn3* binds to LNS domain of  $\beta$ -Nrxns. **A**, diagrams of Nrxn1 $\beta$  and Nrxn1 $\gamma$  constructs used in **B**. **B**, cell surface-binding assays. HEK293T cells expressing FLAG-tagged Nrxn1 $\beta$ <sup>+SS4</sup> WT, its deletion variants ( $\Delta$ HRD,  $\Delta$ LNS, or  $\Delta$ Stalk1), or FLAG-tagged Nrxn1 $\gamma$  WT were incubated with IgClstn3, IgNL-2, or IgC, and analyzed by immunofluorescence imaging for Ig-fusion proteins (red) and FLAG (green). All binding reactions were performed in 2 mM CaCl<sub>2</sub> and 2 mM MgCl<sub>2</sub>. Scale bars: 10  $\mu$ m (applies to all images). **C**, quantification of cell surface binding in **B**. Data are mean  $\pm$  S.E. (\*\*,  $p < 0.01$ ; \*\*\*\*,  $p < 0.0001$ ; nonparametric Kruskal-Wallis test with Dunn's post hoc test; number of cells analyzed = 9–19).  $p$  values for IgC binding: WT versus  $\Delta$ HRD,  $p = 0.0841$ ; WT versus  $\Delta$ LNS,  $p > 0.9999$ ; WT versus  $\Delta$ Stalk1,  $p = 0.1214$ ; WT versus Nrxn1 $\gamma$ ,  $p = 0.0616$ .  $p$  value for IgClstn3 binding: WT versus  $\Delta$ HRD,  $p = 0.9581$ ; WT versus  $\Delta$ LNS,  $p < 0.0001$ ; WT versus  $\Delta$ Stalk1,  $p < 0.0001$ ; WT versus Nrxn1 $\gamma$ ,  $p < 0.0001$ .  $p$  values for IgNL-2 binding: WT versus  $\Delta$ HRD,  $p = 0.4988$ ; WT versus  $\Delta$ LNS,  $p < 0.0001$ ; WT versus  $\Delta$ Stalk1,  $p = 0.0033$ ; WT versus Nrxn1 $\gamma$ ,  $p < 0.0001$ .

1) in contacting axons of co-cultured neurons (Fig. S5), suggesting that *Clstn3* exerts its synaptogenic activities through Nrxn SS4-positive splice variants at both excitatory and inhibitory synapses.

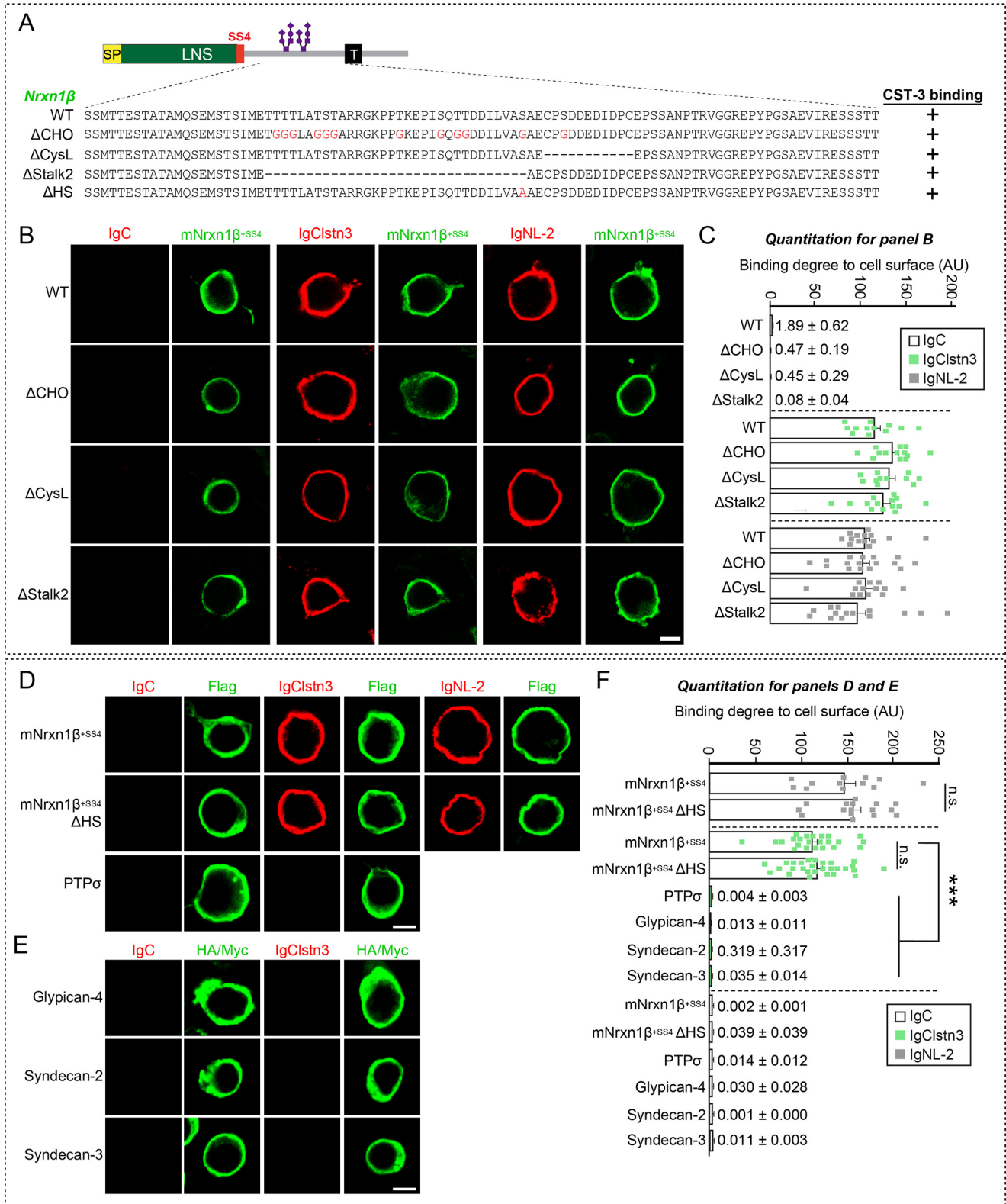
### Generation and characterization of *Clstn3* conditional knockout (cKO) mice

To elucidate the physiological significance of *Clstn3*–Nrxn interactions *in vivo*, we used *Clstn3*<sup>tm1a(EUCOMM)Hmgu</sup> mice in which a targeting cassette harboring FRT, lacZ, and loxP sites was inserted between exon 7 and exon 8, resulting in a “knock-out-first” lacZ-reporter-tagged *Clstn3*<sup>tm1a</sup> insertion allele with conditional potential (21). We then crossed *Clstn3*<sup>tm1a/tm1a</sup> mice with an FLPe knock-in strain to remove contaminating transgenes and the neomycin resistance cassette to generate *Clstn3*<sup>tm1c(EUCOMM)Hmgu</sup> mice. To decide which Cre driver lines to cross, for the current study, we first analyzed *Clstn3* expres-

sion patterns in the mouse brain. For this, we performed RNA-scope-based *in situ* hybridization analysis using a *Clstn3*-specific probe. This analysis showed that *Clstn3* mRNA was strongly expressed in most pyramidal cell layers and interneurons in the mouse hippocampus (Fig. 6A), with particularly prominent expression observed in pyramidal cell layers in the CA3 region (Fig. 6, A and C). We further found that *Clstn3* mRNA was also expressed in parvalbumin (PV)- and somatostatin (SST)-positive GABAergic interneurons in the hippocampus, as previously reported (14) (Fig. 6B). Moreover, immunofluorescence analyses using a *Clstn3*-specific antibody (JK091) showed that the expression pattern of the *Clstn3* protein was similar to that of *Clstn3* mRNA in the hippocampus (Fig. 6D). Based on these results, the Nestin-Cre (Nestin-*Clstn3*) driver line was chosen to further cross with *Clstn3*<sup>tm1c(EUCOMM)Hmgu</sup> mice to generate *Clstn3*-cKO mice (Fig. 7, A and B). Loss of *Clstn3* protein in Nestin-*Clstn3*

mice was verified by the absence of detectable *Clstn3* immunoreactivity to *Clstn3*-specific antibodies (JK091; Fig. 7, G and H, and Fig. S6). These mice were largely indistinguishable from control littermates (*Clstn3*<sup>fl/fl</sup>; Ctrl) in terms of birth rate, although Nestin-*Clstn3* mice weighed marginally (but significantly) less at both postnatal day 30 (P30) and P54, which is a generalized metabolic

phenotype of the Nestin-Cre driver line (Fig. 7C, Table S2). In addition, gross morphology (as assessed by Nissl staining) and neuron numbers (as assessed by NeuN staining) in Nestin-*Clstn3* mice were comparable with those of control littermates (Fig. 7, D–F). Semi-quantitative immunoblot analyses showed that the relative expression levels of various synaptic proteins in the



## Interaction of *Clstn3* with $\alpha/\beta$ -Nrxns

hippocampus (Fig. 7G) and cortex (Fig. 7H) of Nestin-*Clstn3* mice were unchanged compared with littermate controls (Fig. 7, G–I). Collectively, these data suggest that *Clstn3* is not essential for mouse survival or breeding, and does not affect the expression levels of other synaptic proteins.

### Cadherin domains of *Clstn3* are required for restoration of the impaired excitatory innervations observed in *Clstn3*-cKO hippocampal neurons

We next analyzed the effect of *Clstn3* deletion on the intensity of excitatory and inhibitory synaptic puncta in various layers of the hippocampal CA1 region using Nestin-*Clstn3* (Figs. 8 and 9). We found a significant decrease in the intensity of VGLUT1 and PSD-95 (excitatory postsynaptic marker) puncta in most layers of hippocampal CA1 regions (stratum oriens (SO) and stratum radiatum (SR)), but not in the stratum lacunosum moleculare (SLM) layer, in *Clstn3*-cKO (Fig. 8, B–E). In contrast, the intensity of GAD67, GAD65, and GABA<sub>A</sub>R $\gamma$ 2 puncta was unchanged in all examined layers of hippocampal CA1 regions (SO, SR, stratum pyramidale (SP), and SLM) (Fig. 9, A–D). To investigate the physiological significance of *Clstn3*–Nrxn interactions *in vivo*, we constructed AAVs encoding full-length *Clstn3* (Full), cadherin domains plus intracellular regions (Cad), or a cadherin domain-deleted *Clstn3* fragment ( $\Delta$ Cad) (Fig. 8A, Fig. S7). We then stereotactically injected AAVs expressing the indicated *Clstn3* protein into the CA1 hippocampus of ~9-week-old Nestin-*Clstn3* mice and performed quantitative immunofluorescence analyses after 2 weeks using antibodies to VGLUT1 or PSD-95 (Fig. 8, A–E). Expression of *Clstn3* Full restored the decreased VGLUT1 and PSD-95 puncta density to WT mouse levels in SO and SR layers of Nestin-*Clstn3* mice (Fig. 8, B–E). Strikingly, expression of *Clstn3* Cad, but not *Clstn3*  $\Delta$ Cad, also restored the decreased VGLUT1 puncta density in the SR layer, but neither *Clstn3* Cad nor *Clstn3*  $\Delta$ Cad expression exerted a rescue effect in the SO layer of Nestin-*Clstn3* mice (Fig. 8, B–E). These results suggest that *Clstn3* organizes the development of hippocampal CA1 excitatory synapses, and likely acts through cadherin domains-mediated interactions with presynaptic Nrxns to control the specific excitatory synaptic projections involving the SR layer.

To complement these anatomical analyses, we performed whole cell electrophysiological recordings of miniature excitatory and inhibitory postsynaptic currents (mEPSCs and

mIPSCs) in brain slices from Nestin-*Clstn3* and littermate WT mice (Fig. S8). Surprisingly, no differences in the amplitude or frequency of mEPSCs and mIPSCs were detected between Nestin-*Clstn3* and Ctrl mice (Fig. S8). These results suggest that *Clstn3* is not required for basal excitatory synaptic transmission in CA1 hippocampal pyramidal neurons.

## Discussion

The present study was initiated with the goal of reconciling discrepancies surrounding molecular mechanisms of *Clstn3*-mediated synapse development. For this, we revisited the most critical (and controversial) issues using newly engineered Nrxns expression vectors and recombinant proteins, and a newly developed *Clstn3*-cKO mice. Taken together with our previous findings, the three principal observations of the current study provide plausible explanations for discrepancies surrounding the molecular mechanisms of *Clstn3*-mediated synapse development.

First, we found that *Clstn3* binds directly to  $\beta$ -Nrxns (Figs. 1 and 2). This interaction was only detected using newly engineered Nrxn1 $\beta$  constructs that were expressed at ~100-fold higher levels (Figs. 1 and 2; Fig. S1). Because Nrxn1 $\beta$   $\Delta$ Stalk1 displayed a significant decrease binding to *Clstn3* and this juxtamembrane sequence is heavily glycosylated, we initially speculated that glycosylation patterns contributed to *Clstn3* binding (Figs. 2 and 3); however, removal of glycosylated residues did not impair binding (Fig. 4). Instead, we conclude that this sequence may influence the orientation and/or conformation of the LNS domain in a manner that is critical for its interaction with *Clstn3*. Structural studies have suggested that a  $\beta$ -Nrxn LNS domain containing an SS4 insertion exists as a dynamic equilibrium between two conformational states: one in which the splice insert forms a protruded  $\alpha$ -helix that supports binding to cerebellins (Cblns), and one in which the additional residues adopt a  $\beta$ -sheet conformation and restores binding to NLS and LRRTMs (22). Because *Clstn3* exhibits a slight preference for binding SS4–positive Nrxns, it is tempting to speculate that restoration of downstream residues promoted a conformational change in the SS4 insert, leading to *Clstn3* binding. As noted above, the current study, unlike our previous study and that of Pettem *et al.* (14), employed newly engineered Nrxn recombinant proteins to provide the first demonstration of direct interactions with recombinant *Clstn3* proteins (Fig. 2). Moreover, in keeping with results from the current study, it

**Figure 4. No Effect of Nrxn1 $\beta$  O-glycosylation on *Clstn3*–Nrxn1 $\beta$  interactions.** A, diagrams of Nrxn1 constructs used in the cell surface–labeling assays presented in B, B, cell surface–labeling assays. HEK293T cells expressing FLAG-tagged Nrxn1 $\beta$ <sup>554</sup> WT or its deletion variants ( $\Delta$ CHO,  $\Delta$ CysL, or  $\Delta$ Stalk2) were incubated with IgC (control), IgClstn3, or IgNL-2 and analyzed by immunofluorescence imaging for Ig-fusion proteins (red) and FLAG (green). All binding reactions were performed in 2 mM CaCl<sub>2</sub> and 2 mM MgCl<sub>2</sub>. Scale bars: 10  $\mu$ m for all images. C, quantification of cell-surface binding in B. Data are mean  $\pm$  S.E. (number of cells analyzed = 11–16). *p* values for IgC binding: WT versus  $\Delta$ CHO, *p* = 0.0816; WT versus  $\Delta$ CysL, *p* = 0.1732; WT versus  $\Delta$ Stalk2, *p* = 0.0651. *p* value for IgClstn3 binding: WT versus  $\Delta$ CHO, *p* = 0.0724; WT versus  $\Delta$ CysL, *p* = 0.4738; WT versus  $\Delta$ Stalk2, *p* > 0.9999. *p* values for IgNL-2 binding: WT versus  $\Delta$ CHO, *p* > 0.9999; WT versus  $\Delta$ CysL, *p* > 0.9999; WT versus  $\Delta$ Stalk2, *p* > 0.9999. D, cell surface–labeling assays. HEK293T cells expressing FLAG-tagged Nrxn1 $\beta$ <sup>554</sup> WT, its heparan sulfate binding defective mutant ( $\Delta$ HS), or PTP $\sigma$  were incubated with IgC (control), IgClstn3, or IgNL-2 and analyzed by immunofluorescence imaging for Ig-fusion proteins (red) and FLAG (green). All binding reactions were performed in 2 mM CaCl<sub>2</sub> and 2 mM MgCl<sub>2</sub>. Scale bars: 10  $\mu$ m for all images. E, cell surface–labeling assays. HEK293T cells expressing HA-tagged Glypican-4, Myc-tagged Syndecan-2, or Syndecan-3 were incubated with IgC (control), or IgClstn3 and analyzed by immunofluorescence imaging for Ig-fusion proteins (red) and HA/Myc (green). All binding reactions were performed in 2 mM CaCl<sub>2</sub> and 2 mM MgCl<sub>2</sub>. Scale bars: 10  $\mu$ m for all images. F, quantification of cell-surface binding in D and E. Data are mean  $\pm$  S.E. (number of cells analyzed = 12–28). (\*\*\*) *p* < 0.001; nonparametric Kruskal–Wallis test with Dunn’s post hoc test). *p* value for IgNL-2 binding: WT versus  $\Delta$ HS, *p* = 0.3713. *p* value for IgClstn3 binding: WT versus  $\Delta$ HS, *p* > 0.9999; WT versus PTP $\sigma$ , *p* < 0.0001; WT versus Glypican-4, *p* < 0.0001; WT versus Syndecan-2, *p* < 0.0001; WT versus Syndecan-3, *p* < 0.0001. *p* values for IgC binding: WT versus  $\Delta$ HS, *p* > 0.9999; WT versus PTP $\sigma$ , *p* > 0.9999; WT versus Glypican-4, *p* > 0.9999; WT versus Syndecan-2, *p* > 0.9999; WT versus Syndecan-3, *p* = 0.1694.

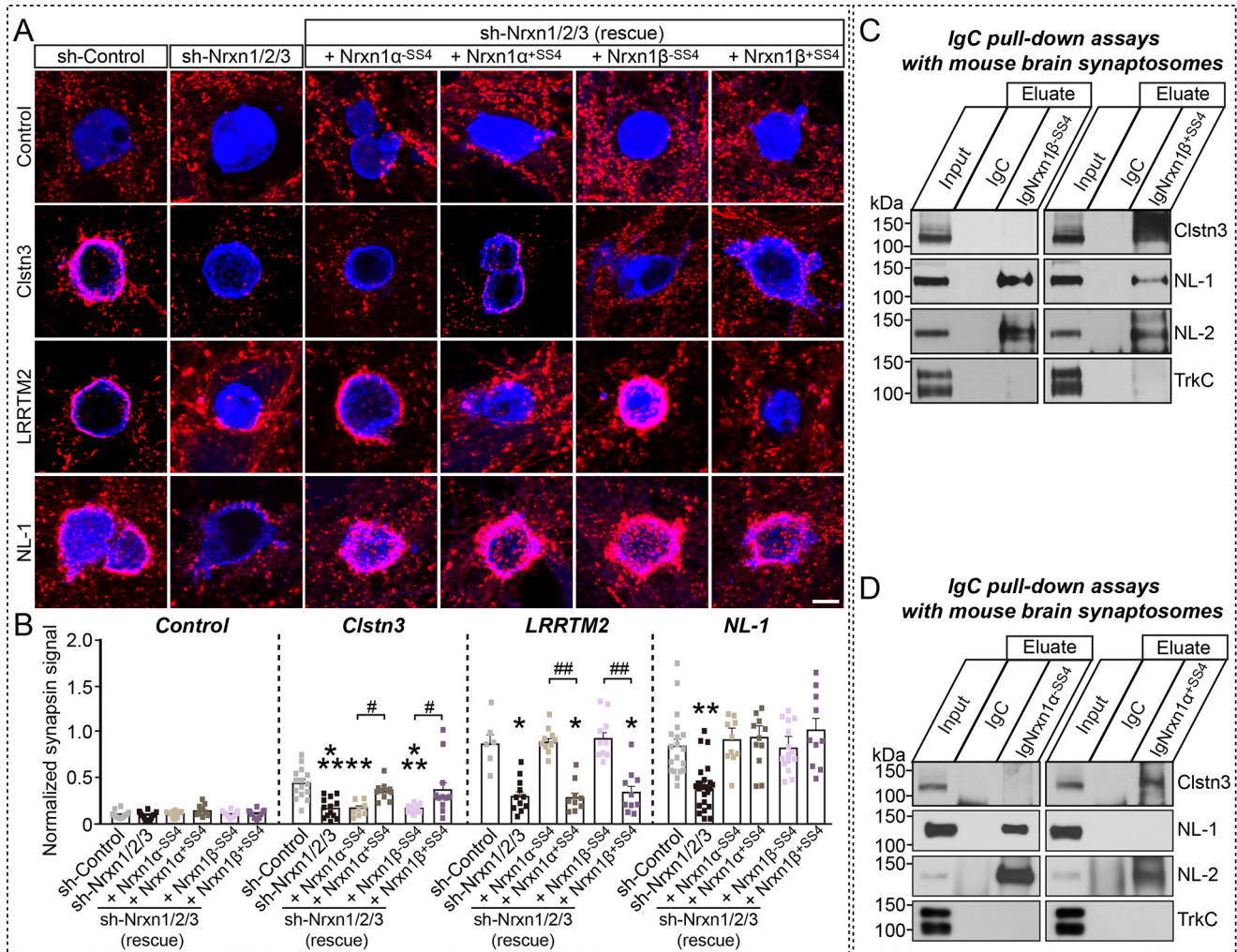


**Figure 5. Selected Nrnx variants are required for Clstn3-mediated induction of presynaptic differentiation.** A and B, effects of Nrnx-TKD (sh-Nrxn1/2/3) on the synaptogenic activities of Clstn3, LRRTM2, and NL-1. HEK293T cells expressing the indicated proteins were co-cultured with neurons infected with control lentiviruses (*sh-Control*) or lentiviruses expressing sh-Nrxn1/2/3, without or with coexpression of the indicated Nrnx1 $\alpha$  or Nrnx1 $\beta$  splice variants. Representative images (A) of co-cultures immunostained with antibodies to mVenus or HA (blue) and synapsin I (red). Scale bar: 10  $\mu$ m (applies to all images). Quantitation (B) of heterologous synapse-formation assays, determined by calculating the ratio of synapsin to EGFP/HA fluorescence signals. Dashed lines correspond to control values used as a baseline. Data are mean  $\pm$  S.E. (\*\*\*)  $p < 0.001$ ; \*\*  $p < 0.01$ ; \*  $p < 0.05$ ; ##  $p < 0.01$ ; #  $p < 0.05$ ; nonparametric Kruskal-Wallis test with Dunn's post hoc test; sh-Control/Control,  $n = 10$ ; sh-Nrxn1/2/3/Control,  $n = 10$ ; sh-Nrxn1/2/3 (rescue + Nrnx1 $\alpha$ <sup>+SS4</sup>)/Control,  $n = 10$ ; sh-Nrxn1/2/3 (rescue + Nrnx1 $\alpha$ <sup>-SS4</sup>)/Control,  $n = 10$ ; sh-Nrxn1/2/3 (rescue + Nrnx1 $\beta$ <sup>+SS4</sup>)/Control,  $n = 10$ ; sh-Nrxn1/2/3 (rescue + Nrnx1 $\beta$ <sup>-SS4</sup>)/Control,  $n = 10$ ; sh-Control/Clstn3,  $n = 15$ ; sh-Nrxn1/2/3/Clstn3,  $n = 13$ ; sh-Nrxn1/2/3 (rescue + Nrnx1 $\alpha$ <sup>+SS4</sup>)/Clstn3,  $n = 8$ ; sh-Nrxn1/2/3 (rescue + Nrnx1 $\alpha$ <sup>-SS4</sup>)/Clstn3,  $n = 11$ ; sh-Nrxn1/2/3 (rescue + Nrnx1 $\beta$ <sup>+SS4</sup>)/Clstn3,  $n = 11$ ; sh-Nrxn1/2/3 (rescue + Nrnx1 $\beta$ <sup>-SS4</sup>)/Clstn3,  $n = 13$ ; sh-Control/LRRTM2,  $n = 6$ ; sh-Nrxn1/2/3/LRRTM2,  $n = 11$ ; sh-Nrxn1/2/3 (rescue + Nrnx1 $\alpha$ <sup>+SS4</sup>)/LRRTM2,  $n = 10$ ; sh-Nrxn1/2/3 (rescue + Nrnx1 $\alpha$ <sup>-SS4</sup>)/LRRTM2,  $n = 9$ ; sh-Nrxn1/2/3 (rescue + Nrnx1 $\beta$ <sup>+SS4</sup>)/LRRTM2,  $n = 10$ ; sh-Nrxn1/2/3 (rescue + Nrnx1 $\beta$ <sup>-SS4</sup>)/LRRTM2,  $n = 9$ ; sh-Nrxn1/2/3 (rescue + Nrnx1 $\alpha$ <sup>+SS4</sup>)/NL-1,  $n = 25$ ; sh-Nrxn1/2/3 (rescue + Nrnx1 $\alpha$ <sup>-SS4</sup>)/NL-1,  $n = 10$ ; sh-Nrxn1/2/3 (rescue + Nrnx1 $\beta$ <sup>+SS4</sup>)/NL-1,  $n = 12$ ; sh-Nrxn1/2/3 (rescue + Nrnx1 $\beta$ <sup>-SS4</sup>)/NL-1,  $n = 10$ .  $p$  values for Control conditions: sh-Control versus sh-Nrxn1/2/3,  $p > 0.9999$ ; sh-Nrxn1/2/3 versus sh-Nrxn1/2/3 (rescue + Nrnx1 $\alpha$ <sup>-SS4</sup>),  $p > 0.9999$ ; sh-Nrxn1/2/3 (rescue + Nrnx1 $\alpha$ <sup>-SS4</sup>) versus sh-Nrxn1/2/3 (rescue + Nrnx1 $\alpha$ <sup>+SS4</sup>),  $p > 0.9999$ ; sh-Nrxn1/2/3 (rescue + Nrnx1 $\beta$ <sup>-SS4</sup>) versus sh-Nrxn1/2/3 (rescue + Nrnx1 $\beta$ <sup>+SS4</sup>),  $p > 0.9999$ .  $p$  values for Clstn3 condition: sh-Control versus sh-Nrxn1/2/3,  $p = 0.003$ ; sh-Control versus sh-Nrxn1/2/3 (rescue + Nrnx1 $\alpha$ <sup>-SS4</sup>),  $p = 0.0026$ ; sh-Control versus sh-Nrxn1/2/3 (rescue + Nrnx1 $\alpha$ <sup>+SS4</sup>),  $p > 0.9999$ ; sh-Control versus sh-Nrxn1/2/3 (rescue + Nrnx1 $\beta$ <sup>-SS4</sup>),  $p = 0.0003$ ; sh-Control versus sh-Nrxn1/2/3 (rescue + Nrnx1 $\beta$ <sup>+SS4</sup>),  $p > 0.9999$ ; sh-Nrxn1/2/3 (rescue + Nrnx1 $\alpha$ <sup>-SS4</sup>) versus sh-Nrxn1/2/3 (rescue + Nrnx1 $\alpha$ <sup>+SS4</sup>),  $p = 0.0427$ ; sh-Nrxn1/2/3 (rescue + Nrnx1 $\beta$ <sup>-SS4</sup>) versus sh-Nrxn1/2/3 (rescue + Nrnx1 $\beta$ <sup>+SS4</sup>),  $p = 0.0123$ .  $p$  values for LRRTM2 condition: sh-Control versus sh-Nrxn1/2/3,  $p = 0.0252$ ; sh-Control versus sh-Nrxn1/2/3 (rescue + Nrnx1 $\alpha$ <sup>-SS4</sup>),  $p > 0.9999$ ; sh-Control versus sh-Nrxn1/2/3 (rescue + Nrnx1 $\alpha$ <sup>+SS4</sup>),  $p = 0.325$ ; sh-Control versus sh-Nrxn1/2/3 (rescue + Nrnx1 $\beta$ <sup>-SS4</sup>),  $p > 0.9999$ ; sh-Control versus sh-Nrxn1/2/3 (rescue + Nrnx1 $\beta$ <sup>+SS4</sup>),  $p = 0.0285$ ; sh-Nrxn1/2/3 (rescue + Nrnx1 $\alpha$ <sup>-SS4</sup>) versus sh-Nrxn1/2/3 (rescue + Nrnx1 $\alpha$ <sup>+SS4</sup>),  $p = 0.0021$ .  $p$  values for NL-1 condition: sh-Control versus sh-Nrxn1/2/3,  $p = 0.0015$ ; sh-Control versus sh-Nrxn1/2/3 (rescue + Nrnx1 $\alpha$ <sup>-SS4</sup>),  $p > 0.9999$ ; sh-Control versus sh-Nrxn1/2/3 (rescue + Nrnx1 $\alpha$ <sup>+SS4</sup>),  $p > 0.9999$ ; sh-Control versus sh-Nrxn1/2/3 (rescue + Nrnx1 $\beta$ <sup>-SS4</sup>),  $p > 0.9999$ ; sh-Control versus sh-Nrxn1/2/3 (rescue + Nrnx1 $\beta$ <sup>+SS4</sup>),  $p > 0.9999$ ; sh-Nrxn1/2/3 (rescue + Nrnx1 $\alpha$ <sup>-SS4</sup>) versus sh-Nrxn1/2/3 (rescue + Nrnx1 $\alpha$ <sup>+SS4</sup>),  $p > 0.9999$ ; sh-Nrxn1/2/3 (rescue + Nrnx1 $\beta$ <sup>-SS4</sup>) versus sh-Nrxn1/2/3 (rescue + Nrnx1 $\beta$ <sup>+SS4</sup>),  $p > 0.9999$ . C and D, pull-down assays in solubilized mouse synaptosomal fractions. Assays were performed using recombinant IgNrxn1 $\beta$  (C), IgNrxn1 $\alpha$  (D), or IgC proteins. Equal amounts of bound proteins were analyzed using the antibodies indicated to the right of panels. Input, 5%.

was previously reported that  $\beta$ 1-Nrxn binds immobilized Clstn3 with a complex binding mode (23). Although it was claimed that Clstn3 interacts with  $\alpha$ -Nrxns (but not  $\beta$ -Nrxns), and we previously failed to detect the interaction of Nrxns with

Clstn3 (14, 15), we would argue that conclusions based on binding experiments employing a limited set of methodologies could unintentionally be misleading, as was the case for our previous report (15).

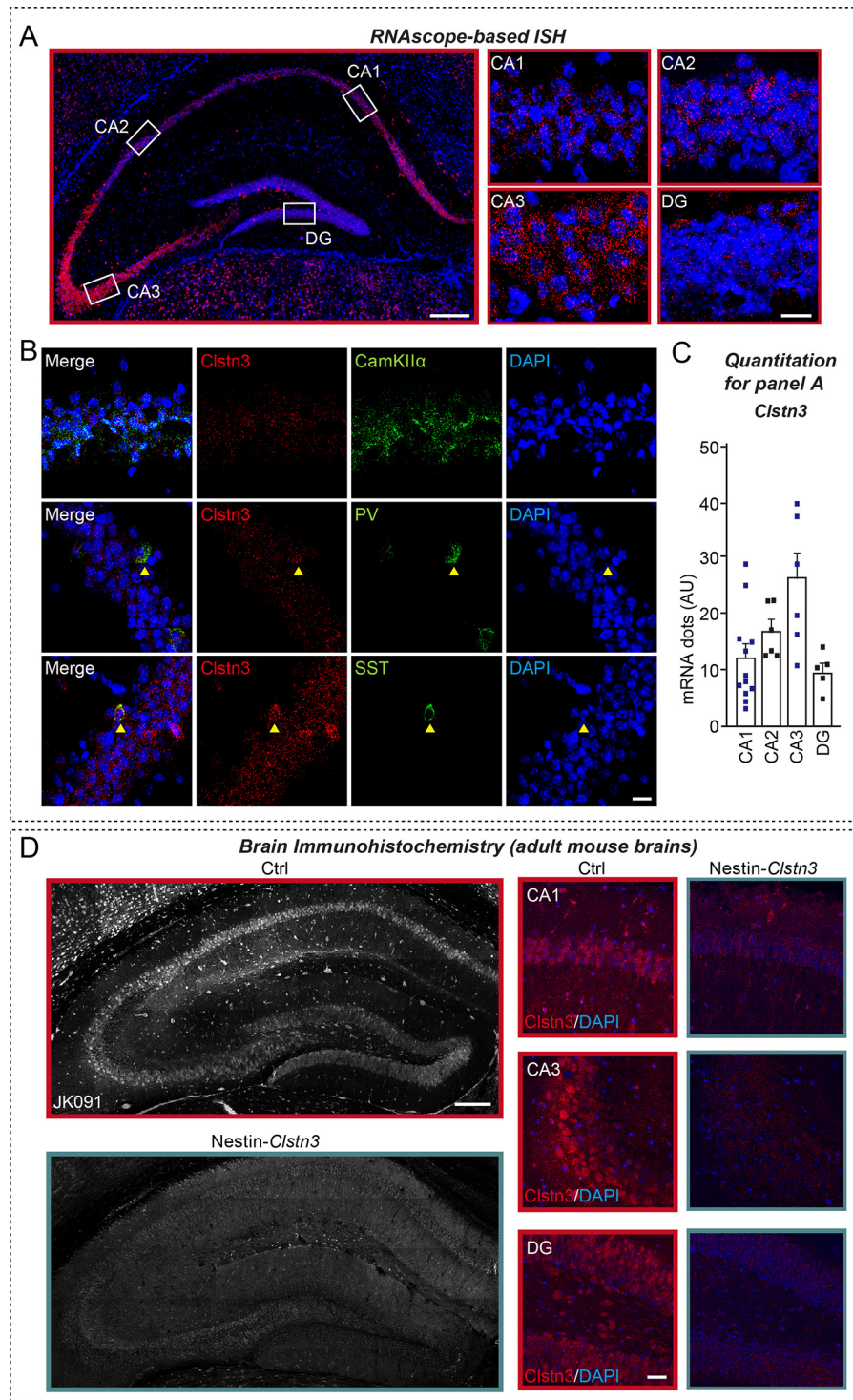


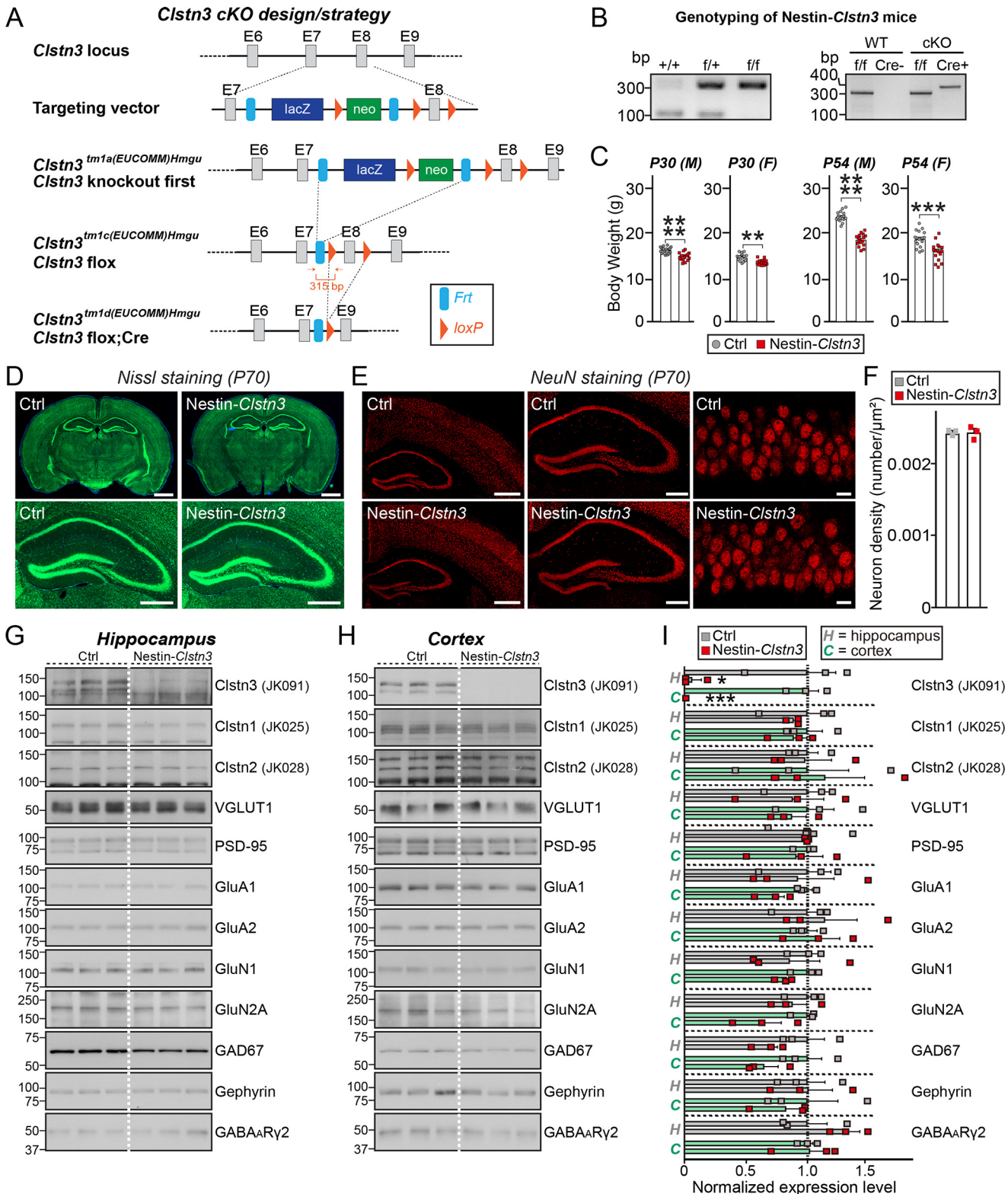
**Figure 6. *Clstn3* is expressed in glutamatergic, PV-positive, and SST-positive neurons in the adult mouse hippocampus.** A-C, expression of *Clstn3* mRNA (red) in various hippocampal regions, as visualized by *in situ* hybridization using RNAscope technology. Nuclei were stained with DAPI (blue). Representative image (A) and quantitative analyses (C) of RNAscope data are shown. Scale bar: 200  $\mu$ m for larger color image on the left, and 20  $\mu$ m for images on the right. B, expression of *Clstn3* mRNA (red) in CamKII $\alpha$ -positive glutamatergic, PV-positive, and SST-positive neurons in hippocampal regions, shown by staining for the indicated gene probes (green) by RNAscope-based *in situ* hybridization, followed by counterstaining with the nuclear dye DAPI (blue). Scale bar: 20  $\mu$ m. D, expression of *Clstn3* protein in the hippocampus of *Clstn3*<sup>flx/flx</sup> (Ctrl) or Nestin-Cre;*Clstn3*<sup>flx/flx</sup> (Nestin-*Clstn3*) mice at P42 (6 weeks), as visualized by immunohistochemistry using anti-*Clstn3* antibodies (JK091). Nuclei were stained with DAPI (blue). Scale bar: 200  $\mu$ m for larger images on the left, and 20  $\mu$ m for images on the right.

Second, re-expressing select Nrxn1 variants in Nrxn-deficient neurons rescued impaired *Clstn3* synaptogenic activity (Fig. 5). Previously, we reported that presynaptic Nrxns serve as

functional receptors for postsynaptic *Clstn3*, but do not directly interact with them (15). Our new data indicate that our previous model should incorporate direct binding of  $\beta$ -Nrxns to

*Clstn3* (Figs. 1–5). In support of this interpretation, BAM-2, a Nrxn-related *Caenorhabditis elegans* homolog, was recently reported to bind CASY-1 and mediate neural circuit wiring of male-specific hook-sensory HOA neurons in *C. elegans* (24). Intriguingly, CASY-1 does not directly interact with NRX-1, a canonical *C. elegans* Nrxn ortholog (24). Although BAM-2

exhibits considerable sequence homology/similarity with  $\alpha$ -Nrxns (25), whether these vertebrate and worm genes are functionally homologous remains to be determined. Nrxns interact with various postsynaptic proteins, including NLs, LRRTMs, Cblns, and latrophilins (3). These interactions are dynamically modulated by the alternative splicing status of



## Interaction of *Clstn3* with $\alpha/\beta$ -Nrxns

Nrxns, mainly at the canonical SS4 splice site. Strikingly, the synapse-promoting activity of *Clstn3* required Nrxn splice variants containing the SS4 insert (Fig. 5), as has been shown for other Nrxn ligands (*i.e.* Cblns) (3). These observations are consistent with slightly stronger binding of  $\text{Nrxn1}\beta^{+SS4}$  to *Clstn3*, which contrasts with the exclusive binding of  $\text{Nrxn1}\beta^{+SS4}$  to Cblns (Fig. 1, *G* and *H*). Pulldown experiments in mouse brains also showed that greater enrichment of *Clstn3* using  $\text{IgNrxn1}\alpha^{+SS4}$  than was obtained using  $\text{IgNrxn1}\alpha^{-SS4}$  (Fig. 5, *C* and *D*) (15). Additionally, the shed ectodomain of *Clstn3* suppresses the synaptogenic activity of NL-2 and LRRTM2, suggesting that *Clstn3* competes with these Nrxn ligands (14). However, LRRTM2 interacts only with Nrxn-SS4-negative splice variants (16), whereas *Clstn3* activity requires Nrxn-SS4-positive splice variants; moreover, a  $\beta$ -Nrxn LNS domain (identical to the sixth LNS domain-sixth LNS domain in  $\alpha$ -Nrxns) is sufficient for *Clstn3* binding. Although we still failed to detect clear interactions of  $\alpha$ -Nrxns with *Clstn3* in cell surface-binding assays, we observed robust  $\text{Nrxn1}\alpha$ -*Clstn3* interactions in brain pulldown and direct binding assays (Figs. 2*E* and 5*D*). It is possible that the surface-binding assays employed here were too stringent to observe this interaction, or the cell surface presentation of  $\alpha$ -Nrxns was not optimal for binding. Thus, we conclude that *Clstn3* binds to both  $\alpha$ - and  $\beta$ -Nrxns through a common LNS domain, but a subset of *Clstn3* synaptic functions might require other unidentified ligands *in vivo*. Moreover, given the activity-dependent regulation of Nrxn alternative splicing at the SS4 site (26), future studies should investigate whether *Clstn3*-Nrxn interactions could be finetuned depending on distinct activity patterns *in vivo*. Furthermore, given a recent report that different SS4-positive splice variants of two different Nrxns ( $\text{Nrxn1}$  versus  $\text{Nrxn3}$ ) differentially control different postsynaptic responses (27), it is possible that *Clstn3* preferentially partners with a specific Nrxn *in vivo*.

Third, re-expressing *Clstn3* cadherin domains was sufficient to completely rescue the impaired excitatory synapse structures in hippocampal CA1 neurons from *Nestin-Clstn3* mice (Fig. 8), but only in the SR layer. In contrast, the structural deficits in other hippocampal CA1 layers were rescued by expression of full-length *Clstn3* protein, but not by expression of partial

*Clstn3* proteins (Fig. 8). Although it is possible that other unidentified proteins could also bind to *Clstn3* cadherin domains, it is likely that presynaptic neurexins and postsynaptic *Clstn3* control the properties of excitatory synapse development in specific Schaffer-collateral projections within the SR layer. A recent paper highlighted the fact that the distinctive features of two different Schaffer-collateral projections differentially regulate mushroom spine density and high-magnitude LTP in the SO layer, organized by heterophilic type II cadherins (28). Moreover, Nrxn genes show differential, but overlapping, isoform- and region-dependent expression in different classes of neurons, and undergo highly distinctive, cell type-specific alternative splicing (29, 30). One plausible scenario would be that CA3 neurons projecting to CA1 neurons in the SR layer, but not the SO layer, express higher levels of SS4-positive Nrxns at their nerve terminals. A recent extensive chromogenic and fluorescent *in situ* hybridization analysis showed that the levels of Nrxn mRNAs in hippocampal subfields are significantly lower in GABAergic neurons than excitatory neurons (31), which might account for preferential deficits on excitatory synapses in CA1 hippocampal regions of *Clstn3* KO mice. Another possible scenario is that major glutamatergic axon fibers of Schaffer-collateral (SC) pathways are targeted to CA1 pyramidal neurons in the SR layer, whereas a subpopulation of axon fibers of SC pathways innervates both bistratified GABAergic interneurons in the SO layer and CA1 pyramidal neurons. Additional studies will also be required to determine the identity of neurons *in vivo* that are responsible for Nrxn-*Clstn3* interactions in other neural circuits inside and outside of the hippocampus. Notably, in stark contrast to the previous report that decreased inhibitory synapse structure and transmission in *Clstn3*-KO mice (14), we found that inhibitory synapses in CA1 hippocampal layers and the cortex were morphologically normal in our *Clstn3*-KO mice (Fig. 9). The reason for this discrepancy is currently unclear, but it is likely that *Clstn* family proteins are functionally redundant in the maintenance of basal synaptic transmission; alternatively, *Clstn3* may be specifically required for certain forms of synaptic plasticity. A notable difference between the study of Pettem *et al.* (14) and the current study is that the former targeted exons 2 and 3 of the mouse *Clstn3* gene, whereas our study targeted exon 8 (Fig. 7). In addition,

**Figure 7. Characterization of *Clstn3*-cKO mice.** *A*, strategy used to generate conditional *Clstn3*<sup>tm1d/tm1d</sup> KO mice. Arrows flanking the neomycin gene and FLP recombinant target (*FRT*) or exon 8 (*E8*) indicate loxP sites. Red arrows indicate forward and reverse primers used for genotyping. Note that lacZ and neomycin cassettes are two separate markers. *B*, PCR genotyping of *Nestin-Cre;Clstn3*<sup>fl/fl</sup> (*Nestin-Clstn3*; cKO). The 400-bp Cre-specific PCR product was detected only in *Nestin-Clstn3* mice. The band size of the *Clstn3* floxed allele was 315 bp. *C*, body weight of *Nestin-Clstn3* and *Clstn3*<sup>fl/fl</sup> (*Ctrl*) mice at P30 and P54. Abbreviations: *F*, female; *M*, male. Data are mean  $\pm$  S.E. (\*\*\*\*,  $p < 0.0001$ ; \*\*\*,  $p < 0.001$ ; \*\*,  $p < 0.01$ ; Mann-Whitney U test). *p* values as follows: P30 (*M*), *Ctrl* versus *Nestin-Clstn3*,  $p < 0.0001$ ; P30 (*F*), *Ctrl* versus *Nestin-Clstn3*,  $p = 0.0013$ ; P45 (*M*), *Ctrl* versus *Nestin-Clstn3*,  $p < 0.0001$ ; P45 (*F*), *Ctrl* versus *Nestin-Clstn3*,  $p = 0.0001$ . *D*, normal gross morphology of the *Nestin-Clstn3* brain at P70, as revealed by Nissl staining. Scale bar: 1 mm (top) and 500  $\mu$ m (bottom). *E*, representative images of NeuN (a neuronal marker) staining from the *Nestin-Clstn3* brain. Normal numbers of neurons (*F*) in hippocampal and cortical regions (left, fore-brain coronal section; middle, hippocampal coronal section; right, hippocampal CA1 stratum pyramidale layer). Scale bar: 1 mm (left), 0.5 mm (middle), and 20  $\mu$ m (right). *F*, summary graphs of NeuN (neuron marker) staining from *E*. Data are mean  $\pm$  S.E. (*Ctrl* versus *Nestin-Clstn3*,  $p > 0.9999$ ,  $n = 3$  mice each after averaging data from 6 sections/mouse; *n.s.*, not significant). *G-I*, representative immunoblots for the hippocampus (*G*) and cortex (*H*) and summary graphs of synaptic protein levels (*I*) in crude synaptosomal fractions of P42 *Ctrl* and *Nestin-Clstn3* brains, analyzed by semi-quantitative immunoblotting (equal amounts of protein (30  $\mu$ g) from crude synaptosomal fractions were loaded). Data are mean  $\pm$  S.E. (\*\*\*,  $p < 0.001$ ; \*,  $p < 0.05$ ; Student's *t* test;  $n = 3$  mice each group). *p* values for hippocampus: *Clstn3*, *Ctrl* versus *Nestin-Clstn3*,  $p = 0.0259$ ; *Clstn1*, *Ctrl* versus *Nestin-Clstn3*,  $p = 0.5963$ ; *Clstn2*, *Ctrl* versus *Nestin-Clstn3*,  $p = 0.9662$ ; *VGLUT1*, *Ctrl* versus *Nestin-Clstn3*,  $p = 0.7262$ ; *PSD-95*, *Ctrl* versus *Nestin-Clstn3*,  $p = 0.4220$ ; *GluA1*, *Ctrl* versus *Nestin-Clstn3*,  $p = 0.8297$ ; *GluA2*, *Ctrl* versus *Nestin-Clstn3*,  $p = 0.6194$ ; *GluN1*, *Ctrl* versus *Nestin-Clstn3*,  $p = 0.6259$ ; *GluN2A*, *Ctrl* versus *Nestin-Clstn3*,  $p = 0.4662$ ; *GAD67*, *Ctrl* versus *Nestin-Clstn3*,  $p = 0.1273$ ; *Gephyrin*, *Ctrl* versus *Nestin-Clstn3*,  $p = 0.9630$ ; *GABA<sub>A</sub>R $\gamma$ 2*, *Ctrl* versus *Nestin-Clstn3*,  $p = 0.1533$ , *p* values for cortex: *Clstn3*, *Ctrl* versus *Nestin-Clstn3*,  $p = 0.0005$ ; *Clstn1*, *Ctrl* versus *Nestin-Clstn3*,  $p = 0.5330$ ; *Clstn2*, *Ctrl* versus *Nestin-Clstn3*,  $p = 0.7626$ ; *VGLUT1*, *Ctrl* versus *Nestin-Clstn3*,  $p = 0.6513$ ; *PSD-95*, *Ctrl* versus *Nestin-Clstn3*,  $p = 0.6915$ ; *GluA1*, *Ctrl* versus *Nestin-Clstn3*,  $p = 0.0533$ ; *GluA2*, *Ctrl* versus *Nestin-Clstn3*,  $p = 0.6495$ ; *GluN1*, *Ctrl* versus *Nestin-Clstn3*,  $p = 0.1727$ ; *GluN2A*, *Ctrl* versus *Nestin-Clstn3*,  $p = 0.1004$ ; *GAD67*, *Ctrl* versus *Nestin-Clstn3*,  $p = 0.1180$ ; *Gephyrin*, *Ctrl* versus *Nestin-Clstn3*,  $p = 0.5918$ ; *GABA<sub>A</sub>R $\gamma$ 2*, *Ctrl* versus *Nestin-Clstn3*,  $p = 0.8711$ .

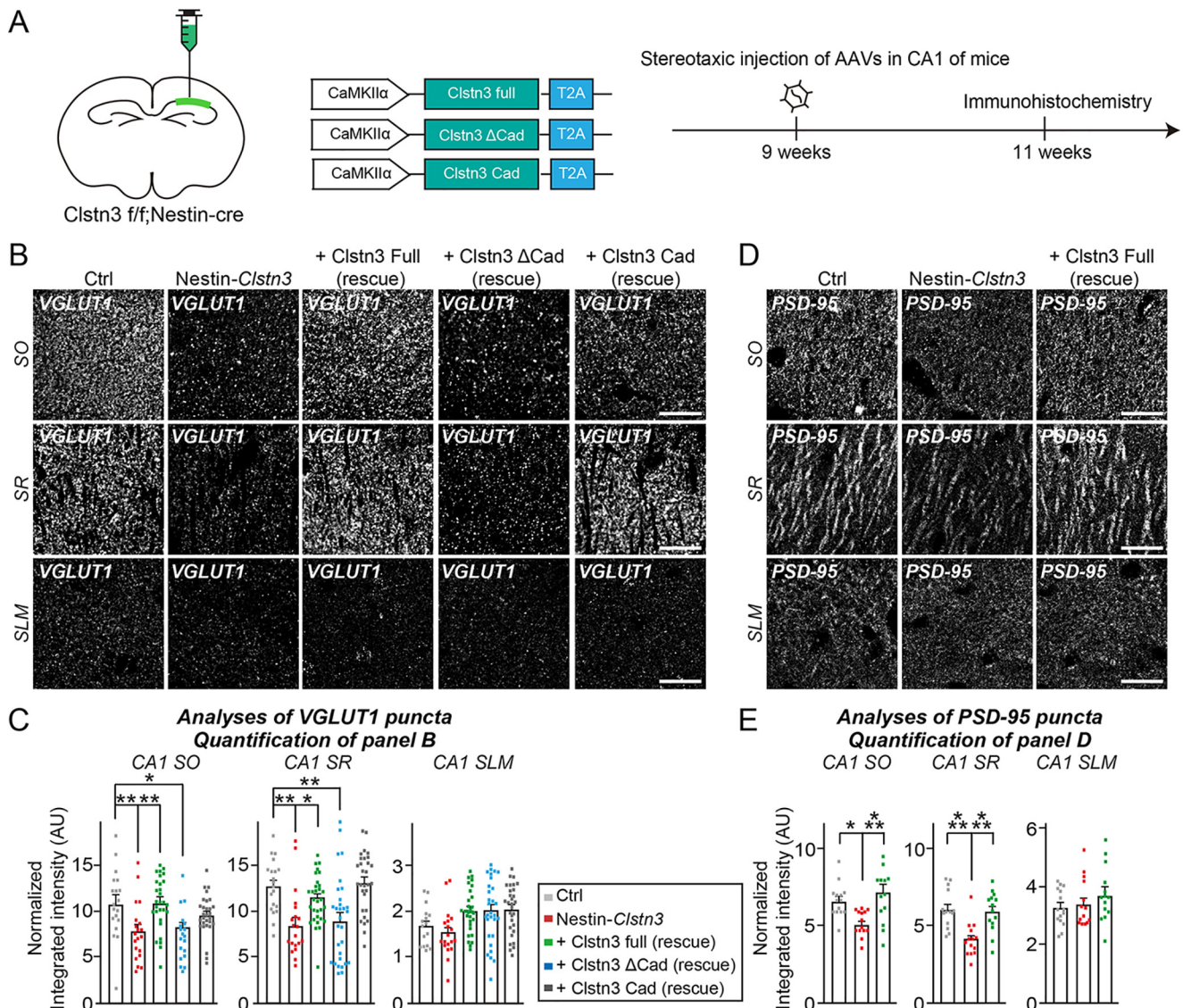


**Figure 8. Interactions of *Clstn3* via its cadherin domains with Nrxns are involved in *Clstn3*-mediated regulation of specific excitatory Schaffer-collateral projections in the CA1 hippocampal region.** *A*, experimental protocols for quantitative immunohistochemistry experiments presented in *B–E*. Quantitative immunohistochemical analyses were performed 2 weeks after stereotaxic injection of the indicated AAVs into the CA1 hippocampal regions of ~9-week-old Nestin-*Clstn3* mice. *B* and *D*, representative images of hippocampal CA1 SO, SR, and SLM regions 2 weeks after stereotaxic injections of the indicated AAVs into *Clstn3*<sup>*fl/fl*</sup> (Ctrl) or Nestin-*Clstn3* mice, followed by immunostaining for the excitatory synapse marker VGLUT1 (*B*) or PSD-95 (*D*). Scale bar: 20  $\mu$ m (applies to all images). *C* and *E*, quantification of the integrated intensity of VGLUT1-positive (*C*) or PSD-95-positive (*E*) synaptic puncta. Data are mean  $\pm$  S.E. (\*,  $p < 0.05$ ; \*\*,  $p < 0.01$ ; \*\*\*,  $p < 0.001$ ; ANOVA with Tukey's test;  $n = 5$  mice each after averaging data from 4 to 6 sections/mouse).  $p$  values for VGLUT1 in CA1 SO: Ctrl versus Nestin-*Clstn3*,  $p = 0.0075$ ; Ctrl versus Clstn3 Full (rescue),  $p > 0.9999$ ; Ctrl versus Clstn3  $\Delta$ Cad (rescue),  $p = 0.0166$ ; Ctrl versus Clstn3 Cad (rescue),  $p > 0.9999$ ; Nestin-*Clstn3* versus Clstn3 full (rescue),  $p = 0.0011$ .  $p$  values for VGLUT1 in CA1 SR: Ctrl versus Nestin-*Clstn3*,  $p = 0.0021$ ; Ctrl versus Clstn3 full (rescue),  $p = 0.7147$ ; Ctrl versus Clstn3  $\Delta$ Cad (rescue),  $p = 0.0028$ ; Ctrl versus Clstn3 Cad (rescue),  $p = 0.9921$ ; Nestin-*Clstn3* versus Clstn3 Full (rescue),  $p = 0.0359$ .  $p$  values for VGLUT1 in CA1 SLM: Ctrl versus Nestin-*Clstn3*,  $p > 0.9999$ ; Ctrl versus Clstn3 Full (rescue),  $p > 0.9999$ ; Ctrl versus Clstn3  $\Delta$ Cad (rescue),  $p > 0.9999$ ; Ctrl versus Clstn3 Cad (rescue),  $p > 0.9999$ .  $p$  values for PSD-95 in CA1 SO: Ctrl versus Nestin-*Clstn3*,  $p = 0.0266$ ; Ctrl versus Clstn3 full (rescue),  $p = 0.4300$ ; Nestin-*Clstn3* versus Clstn3 Full (rescue),  $p = 0.0009$ .  $p$  values for PSD-95 in CA1 SR: Ctrl versus Nestin-*Clstn3*,  $p = 0.0002$ ; Ctrl versus Clstn3 Full (rescue),  $p = 0.8762$ ; Nestin-*Clstn3* versus Clstn3 Full (rescue),  $p = 0.0010$ .  $p$  values for PSD-95 in CA1 SLM: Ctrl versus Nestin-*Clstn3*,  $p = 0.9397$ ; Ctrl versus Clstn3 Full (rescue),  $p = 0.3147$ ; Nestin-*Clstn3* versus Clstn3 Full (rescue),  $p = 0.4975$ .

Pettem *et al.* (14) employed an EIIa-Cre driver line that permits germ line deletion in both excitatory and inhibitory neurons by driving expression of Cre recombinase in the early mouse embryo, whereas we used a pan-neuronal Nestin-Cre driver line that was presumed to be similar to EIIa-Cre. It is also possible that specifically deleting *Clstn3* in GABAergic inhibitory neurons may produce marked deficits in GABAergic synapse development, as previously documented (14), but this did not clearly manifest in our *Clstn3*-cKO mice. A more system-

atic, follow-up investigation to probe cell type-specific contributions of *Clstn3* to distinct anatomical and electrophysiological phenotypes should address these important, but puzzling, observations. Future studies should also probe how Nrxn-*Clstn3* complexes mediate synaptic specificity involving the SR layer of the hippocampal CA1 region. A complete understanding of how *Clstn3* functions will also require investigation of the potential contributions of other *Clstn3* domains (e.g. LNS domain, intracellular region) to

## Interaction of *Clstn3* with $\alpha/\beta$ -Nrxns

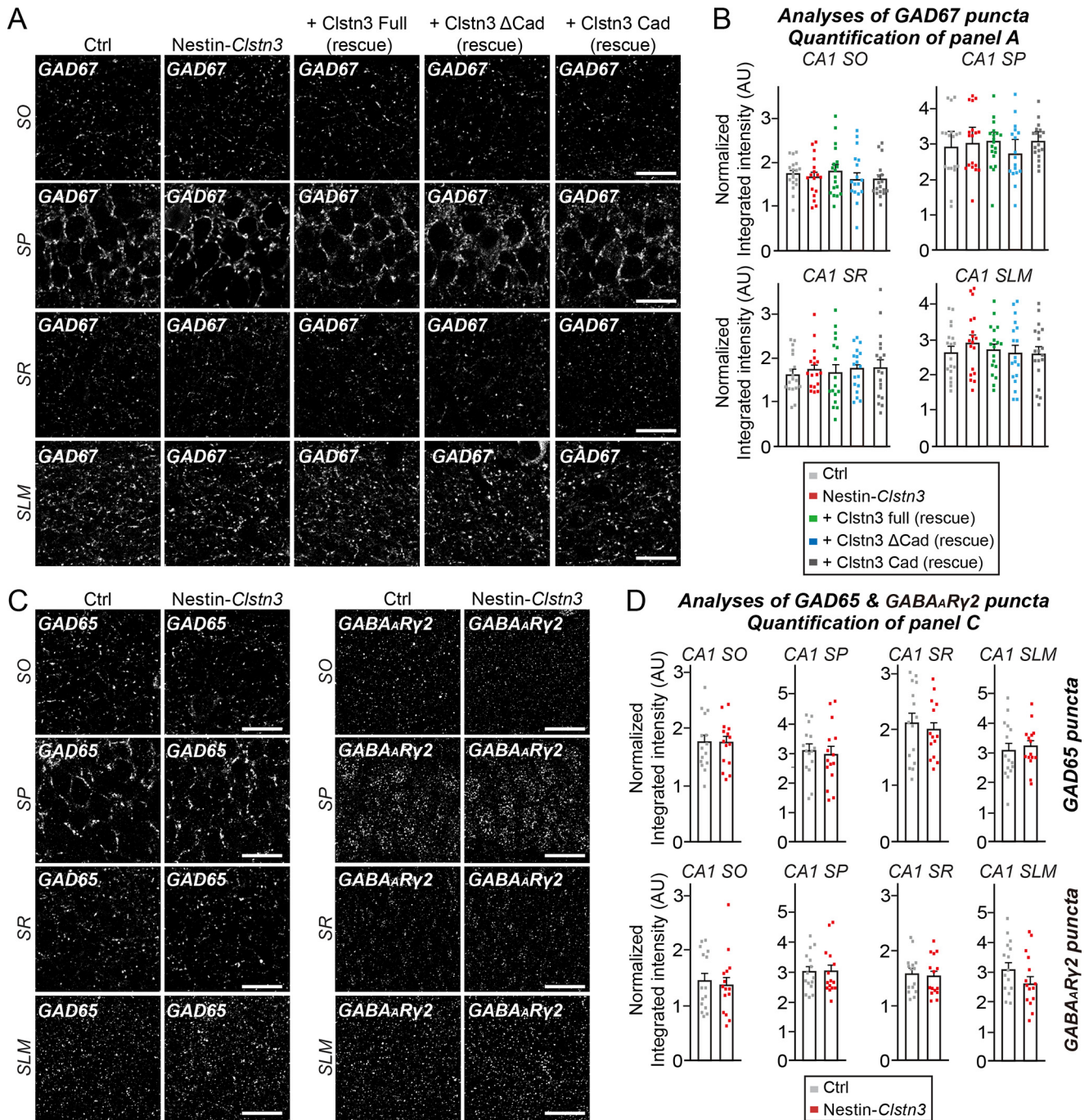


**Figure 9. *Clstn3* deletion does not affect inhibitory synapse development.** *A*, representative images of hippocampal CA1 SO, SP, SR, and SLM regions 2 weeks after stereotactic injection of the indicated AAVs into *Clstn3*<sup>fl/fl</sup> or Nestin-*Clstn3* mice, followed by immunostaining for GABAergic synapse marker (*GAD67*). Scale bar: 20  $\mu$ m (applies to all images). *B*, quantification of the integrated intensity of *GAD67*-positive synaptic puncta. Data are mean  $\pm$  S.E. (ANOVA with Tukey's test;  $n = 5$  mice each after averaging data from 4–6 sections/mouse).  $p$  values for *GAD67* in CA1 SO: Ctrl versus Nestin-*Clstn3*,  $p = 0.9953$ ; Ctrl versus *Clstn3* Full (rescue),  $p = 0.9909$ ; Ctrl versus *Clstn3*  $\Delta$ Cad (rescue),  $p = 0.9141$ ; Ctrl versus *Clstn3* Cad (rescue),  $p = 0.9036$ .  $p$  values for *GAD67* in CA1 SP: Ctrl versus Nestin-*Clstn3*,  $p = 0.9848$ ; Ctrl versus *Clstn3* Full (rescue),  $p = 0.9596$ ; Ctrl versus *Clstn3*  $\Delta$ Cad (rescue),  $p = 0.9478$ ; Ctrl versus *Clstn3* Cad (rescue),  $p = 0.9560$ .  $p$  values for *GAD67* in CA1 SR: Ctrl versus Nestin-*Clstn3*,  $p = 0.9807$ ; Ctrl versus *Clstn3* Full (rescue),  $p > 0.9999$ ; Ctrl versus *Clstn3*  $\Delta$ Cad (rescue),  $p = 0.9837$ ; Ctrl versus *Clstn3* Cad (rescue),  $p = 0.9357$ .  $p$  values for *GAD67* in CA1 SLM: Ctrl versus Nestin-*Clstn3*,  $p = 0.8416$ ; Ctrl versus *Clstn3* Full (rescue),  $p = 0.9981$ ; Ctrl versus *Clstn3*  $\Delta$ Cad (rescue),  $p > 0.9999$ ; Ctrl versus *Clstn3* Cad (rescue),  $p > 0.9999$ . *C*, representative images of hippocampal CA1 SO, SP, SR, and SLM regions in *Clstn3*<sup>fl/fl</sup> or Nestin-*Clstn3* mice, followed by immunostaining for the indicated GABAergic synapse markers (*GAD65* or *GABA<sub>A</sub>R $\gamma$ 2*). Scale bar: 20  $\mu$ m (applies to all images). *D*, quantification of the integrated intensity of *GAD65*- or *GABA<sub>A</sub>R $\gamma$ 2*-positive synaptic puncta. Data are mean  $\pm$  S.E. (nonparametric Kruskal-Wallis test with Dunn's *post hoc* test;  $n = 5$  mice each after averaging data from 4 to 6 sections/mouse).

the functions of *Clstn3*, as was similarly shown in *C. elegans* (24, 32, 33). In summary, the present study unambiguously establishes that *Clstn3* plays a role in specifying the proper-

ties of a specific hippocampal CA1 neural circuit, in part by regulating excitatory synapse development through formation of physical complexes with specific Nrxn splice variants.

## Experimental procedures

### Plasmids

Nrxn rescue vectors were generated by PCR amplification of full-length sequences of mouse *Nrxn1 $\beta$* <sup>SS4</sup>, *Nrxn1 $\beta$* <sup>+SS4</sup>, rat *Nrxn1 $\beta$* <sup>SS4</sup>, rat *Nrxn1 $\beta$* <sup>+SS4</sup>, bovine *Nrxn1 $\alpha$* <sup>SS4</sup>, and bovine *Nrxn1 $\alpha$* <sup>+SS4</sup>, followed by digestion with *NheI* and *BsrGI* and cloning into the TKD vector (L-313 vector). Three nucleotides (underlined) in the GTGCCCTTCCTCTATGACAACT sequence were then mutated to render it small hairpin RNA-resistant. pGW1-FLAG-m*Nrxn1 $\beta$* <sup>SS4</sup> and pGW1-FLAG-m*Nrxn1 $\beta$* <sup>±SS4</sup> were generated by PCR amplification of full-length m*Nrxn1 $\beta$* <sup>SS4</sup> and m*Nrxn1 $\beta$* <sup>+SS4</sup>, respectively, digestion with *KpnI* and *EcoRI*, and cloning into a modified pGW1 vector containing a mouse *Clstn1* signal peptide and FLAG epitope (pGW1 vector; British Biotechnology, Oxford, UK). pCMV-IgC-m*Nrxn1 $\beta$* <sup>SS4</sup> and pCMV-IgC-m*Nrxn1 $\beta$* <sup>±SS4</sup> were generated by PCR amplification of the indicated extracellular regions of m*Nrxn1 $\beta$* <sup>SS4</sup> (aa 1–359) and m*Nrxn1 $\beta$* <sup>+SS4</sup> (aa 1–389), respectively, followed by digestion with *EcoRI* and *Sall* and cloning into a pCMV-IgC vector. pGW1-FLAG-*Clstn3* and pGW1-FLAG-*Clstn3*- $\Delta$ CAD were generated by PCR amplification of full-length mouse *Clstn3* and a *Clstn3* fragment (aa 258–956), respectively, followed by digestion with *KpnI* and *EcoRI* and cloning into the pGW1-FLAG vector. pGW1-FLAG-*Clstn3*-Cad used in Fig. 2A was generated by PCR amplification of two *Clstn3* fragments (aa 29–252 and 848–956), followed by digestion with *KpnI* and *EcoRI* for the first fragment and *EcoRI* only for the second fragment, and subsequent cloning into the pGW1-FLAG vector. The following deletion constructs of m*Nrxn1 $\beta$*  were generated using pGW1-FLAG-m*Nrxn1 $\beta$* <sup>+SS4</sup>: pGW1-FLAG-m*Nrxn1 $\beta$* - $\Delta$ LNS6 was generated by PCR amplification of m*Nrxn1 $\beta$*  (aa 293–468), followed by digestion with *KpnI* and *EcoRI* and cloning into the pGW1-FLAG vector. pGW1-FLAG-m*Nrxn1 $\beta$* - $\Delta$ Stalk1 was generated by PCR amplification of two m*Nrxn1 $\beta$*  fragments (aa 1–315 and 347–468), followed by digestion with *KpnI* and *EcoRI* for the first fragment and *EcoRI* for the second fragment, and subsequent cloning into the pGW1-FLAG vector. pGW1-FLAG-m*Nrxn1 $\beta$* - $\Delta$ Stalk2 was generated by PCR amplification of two m*Nrxn1 $\beta$*  fragments (aa 1–298 and 388–468), followed by digestion with *KpnI* and *EcoRI* for the first fragment and *EcoRI* only for the second fragment, and subsequent cloning into the pGW1-FLAG vector. pGW1-FLAG-m*Nrxn1 $\beta$* - $\Delta$ CysL and pGW1-FLAG-m*Nrxn1 $\beta$* - $\Delta$ CHO were modified from the previously described m*Nrxn1 $\beta$*  point mutants (see Ref. 19 and Fig. 2) by replacing aa 299–468 of WT m*Nrxn1 $\beta$*  with the identical region from the mutated m*Nrxn1 $\beta$*  and cloning the resulting sequence into the pGW1-FLAG vector using *Sall* and *EcoRI* sites. pGW1-FLAG-m*Nrxn1 $\beta$* - $\Delta$ HRD was generated by PCR amplification of m*Nrxn1 $\beta$*  (aa 84–468), followed by digestion with *KpnI* and *EcoRI* and cloning into the pGW1-FLAG vector. pCAGG-m*Nrxn1 $\beta$* <sup>±SS4</sup>-FLAG- $\Delta$ H<sub>S</sub>, L-313-m*Nrxn1 $\beta$* <sup>SS4</sup>- $\Delta$ H<sub>S</sub>-FLAG, and L-313-m*Nrxn1 $\beta$* <sup>±SS4</sup>- $\Delta$ H<sub>S</sub>-FLAG were generated by site-directed mutagenesis to change a single amino acid from ILV $\underline{A}$ S $\underline{A}$ EC $\underline{P}$  to ILV $\underline{A}$ A $\underline{A}$ EC $\underline{P}$  (underlined residues denote the changed residue) using pCAGG-m*Nrxn1 $\beta$* <sup>+SS4</sup>-FLAG, L-313-m*Nrxn1 $\beta$* <sup>SS4</sup>-FLAG, and L-313-m*Nrxn1 $\beta$* <sup>+SS4</sup>-FLAG as templates, respectively. pGW1-FLAG-m*Nrxn1 $\gamma$*  was gen-

erated by PCR amplification of full-length m*Nrxn1 $\gamma$* , followed by digestion with *KpnI* and *EcoRI* and cloning into the pGW1-FLAG vector. Constructs of the extracellular domain of mouse *Clstn3* (*Clstn3* ecto: aa 21–846; *Clstn3* Cad: aa 21–269; *Clstn3*  $\Delta$ CAD: aa 258–846) used in Fig. 2D were N terminally fused to a His<sub>6</sub> tag and HA tag and cloned into the pCAGGS vector using *EcoRI* and *NotI* restriction enzymes. The following constructs were previously described: L-315-Nrxn-TKD (20); pCMV5-mVenus-NL-1 (34); pCMV-IgC-*Clstn3* (15); pCMV-IgC-NL-2 (34); pDisplay-LRRTM2 (35); pCAGG-m*Nrxn1 $\alpha$* <sup>SS4</sup>-FLAG, pCAGG-m*Nrxn1 $\alpha$* <sup>±SS4</sup>-FLAG, pCAGG-m*Nrxn1 $\beta$* <sup>SS4</sup>-FLAG, pCAGG-m*Nrxn1 $\beta$* <sup>±SS4</sup>-FLAG, pCMV-IgC-m*Nrxn1 $\alpha$* <sup>SS4</sup>, and pCMV-IgC-m*Nrxn1 $\alpha$* <sup>±SS4</sup> (36). pAAV<sub>2</sub>-CAG-*Clstn3* Full, pAAV<sub>2</sub>-CAG-*Clstn3* Cad, and pAAV<sub>2</sub>-CAG-*Clstn3*  $\Delta$ Cad were generated by PCR amplification using pGW1-FLAG-*Clstn3* Full, pGW1-FLAG-*Clstn3* Cad, and pGW1-Flag-*Clstn3*  $\Delta$ Cad as templates, respectively, followed by digestion with *EcoRV* and *HindIII* and cloning into a pAAV<sub>2</sub>-CAG vector.

### Antibodies

Fusion proteins of GSH-S-transferase and mouse *Clstn3* (JK091; aa 21–244) were produced in BL21 *Escherichia coli* and purified using a GSH-Sepharose column (GE Healthcare, Chicago, IL, USA). *Clstn1* peptides (JK025; CHQRT-MRDQDTGKEN) and *Clstn2* peptides (JK028; CSSQS-PERSTWNTAGVINIWK) were synthesized and conjugated to keyhole limpet hemocyanin through a cysteine added to the N terminus of the peptide. Following immunization, rabbits with the immunogen antibodies were affinity-purified using a Sulfolink column (Pierce). The following commercially available antibodies were used: mouse monoclonal anti-HA (clone HA-7; Covance), mouse monoclonal anti-FLAG M2 (Sigma-Aldrich), rabbit polyclonal anti-FLAG (Sigma-Aldrich), goat polyclonal anti-EGFP (Rockland Immunochemicals), mouse monoclonal anti-NL-1 (clone N97A/31; NeuroMab), rabbit polyclonal anti-NL-2 (Synaptic Systems, Göttingen, Germany), rabbit monoclonal anti-TrkC (clone C44H5; Cell Signaling Technology), guinea pig polyclonal anti-VGLUT1 (Millipore), mouse monoclonal anti-GAD67 (clone 1G10.2; Millipore), mouse monoclonal anti-PSD-95 (clone K28/43; Thermo Fisher Scientific), mouse monoclonal anti- $\beta$ -actin (clone AC-74; Sigma-Aldrich), mouse monoclonal anti-parvalbumin (clone PARV-19; Millipore), mouse monoclonal anti-gephyrin (clone 3B11; Synaptic Systems), rabbit polyclonal anti-GABA<sub>A</sub> receptor  $\gamma$ 2 (Synaptic Systems); mouse monoclonal anti-GluN1 (clone 54.1; Millipore), rabbit polyclonal anti-GluN2A (Millipore), rabbit polyclonal anti-GluN2B (Millipore), goat anti-human IgG-peroxidase (Sigma-Aldrich), and mouse monoclonal anti-NeuN (clone A60; Millipore). The following antibodies have been previously described: anti-PSD-95 (JK016) (20), anti-synapsin (JK014) (37), anti-GAD65 (JK158) (38), anti-*Clstn3* (JK001) (15), anti-GluA1 (1193) (39), and anti-GluA2 (1195) (39).

### Animals

*Clstn3*<sup>tm1a(ELICOMM)Hmgu</sup> mice, in which a targeting cassette harboring FRT, lacZ, and loxP sites is inserted between exon 7

## Interaction of *Clstn3* with $\alpha/\beta$ -Nrxns

and exon 8, resulting in a “knockout-first” lacZ reporter-tagged *Clstn3*<sup>tm1a</sup> insertion allele with conditional potential, were obtained from the European Mouse Mutagenesis Consortium (EUCOMM). To generate conditional *Clstn3* KO mice (*Clstn3*<sup>fllox/fllox</sup>), we first bred *Clstn3*<sup>tm1a/tm1a</sup> mice in a C57BL/6J background with FLPO recombinase driver mice (C57BL/6N-Tg(CAG-Flpo)1Afst/Mmucd, MMRRC) to generate *Clstn3*<sup>tm1c/tm1c</sup> mice. Male homozygous *Clstn3*<sup>tm1c/tm1c</sup> mice in a C57BL/6J genetic background were crossed with female heterozygous *Clstn3*<sup>tm1c/+</sup> mice (for Nestin conditional) carrying the Cre transgene. A Nestin-Cre (003771) line in a C57BL/6N genetic background, generated by crossing the original Cre-driver lines purchased from the Jackson Laboratory with C57BL/6J for more than five generations, was obtained from Dr. Albert Chen (DUKE-NUS, Singapore). Cre-negative *Clstn3*<sup>fllox/fllox</sup> littermates were used as controls in all experiments. Mice were housed and bred at the animal facility of Daegu Gyeongbuk Institute of Science and Technology (DGIST), and experimental use was approved by the Institutional Animal Care and Use Committee of DGIST (DGIST-IACUC-19052110-00). Mice were given *ad libitum* access to food and water, and were maintained in a controlled environment with a 12-h light/dark cycle. Mice were weaned at the age of P24–27, and mixed-genotype littermate mice were group-housed (4–5 mice per cage) until experiments. Genotyping was performed on genomic DNA extracted from tail biopsies using the 2 $\times$  Taq PCR Smart mix 2 kit (Solgent Co.). Genotyping primers were as follows: *Clstn3* forward, 5'-ACT TGA TCA GTC CTC CTG CAT CAG-3'; *Clstn3* reverse, 5'-CTG AAG TTC AGG GTC AGC CTG TAA-3'; FRT reverse, 5'-CCT TCC TCC TAC ATA GTT GGC AGT-3'; Cre (Nestin-Cre) forward, 5'-CCG CTT CCG CTG GGT CAC TGT-3'; WT reverse, 5'-CTG AGC AGC TGG TTC TGC TCC T-3'; and Cre (Nestin-Cre) reverse, 5'-GAC CGG CAA ACG GAC AGA AGC A-3'. A PCR product of ~130 base pairs (bp) was obtained from WT DNA, whereas *Clstn3*<sup>fllox</sup> produced a PCR product of ~300 bp. The Cre transgene from the Nestin-cre mouse produced a PCR product of ~400 bp.

### Production of recombinant lentiviruses and adeno-associated viruses (rAAVs)

**Lentivirus production**—Recombinant lentiviruses were produced as previously described (34). In brief, HEK293T cells were transfected with three plasmids: lentivirus vectors, psPAX2, and pMD2G, at a 2:2:1 ratio using Lipofectamine 2000 (Thermo Fisher Scientific) according to the manufacturer's protocol. After 72 h, lentiviruses were harvested by collecting the medium from transfected HEK293T cells and briefly centrifuging at 1,000  $\times$  g to remove cellular debris. Filtered media containing 5% sucrose were centrifuged at 117,969  $\times$  g for 2 h; supernatants were then removed and the virus pellet was washed with ice-cold PBS and resuspended in 80  $\mu$ l of PBS.

**AAV production**—HEK293T cells were co-transfected with the indicated AAV vectors and pHelper and pRC1-DJ vectors. Seventy-two h later, transfected HEK293T cells were collected, lysed, and mixed with 40% PEG and 2.5 M NaCl, and centrifuged at 2,000  $\times$  g for 30 min. The cell pellets were resuspended

in HEPES buffer (20 mM HEPES; 115 mM NaCl, 1.2 mM CaCl<sub>2</sub>, 1.2 mM MgCl<sub>2</sub>, 2.4 mM KH<sub>2</sub>PO<sub>4</sub>) and an equal volume of chloroform was added. The mixture was centrifuged at 400  $\times$  g for 5 min, and concentrated three times with a Centriprep centrifugal filter (Millipore) at 1,220  $\times$  g for 5 min each and with an Amicon Ultra centrifugal filter (Millipore) at 16,000  $\times$  g for 10 min. Before titering AAVs, contaminating plasmid DNA was eliminated by treating 1  $\mu$ l of concentrated, sterile-filtered AAVs with 1  $\mu$ l of DNase I (Sigma-Aldrich) for 30 min at 37  $^{\circ}$ C. After treatment with 1  $\mu$ l of stop solution (50 mM EDTA) for 10 min at 65  $^{\circ}$ C, 10  $\mu$ g of protease K (Sigma-Aldrich) was added and AAVs were incubated for 1 h at 50  $^{\circ}$ C. Reactions were inactivated by incubating samples for 20 min at 95  $^{\circ}$ C. The final virus titer was quantified by quantitative RT-PCR detection of EGFP sequences and subsequent reference to a standard curve generated using the pAAV-U6-EGFP plasmid. All plasmids were purified using a Plasmid Maxi Kit (Qiagen GmbH).

### In-gel digest

Gel bands were excised, after which proteins in bands were reduced by treating with DTT, alkylated by treating with indole-3 acetic acid, and then digested by treating with trypsin. Specifically, bands were washed with 10 mM ammonium bicarbonate and 50% acetonitrile, swollen in digestion buffer containing 50 mM ammonium bicarbonate, 5 mM CaCl<sub>2</sub>, and 1  $\mu$ g of trypsin, and then incubated at 37  $^{\circ}$ C for 16 h. Peptides were recovered by two cycles of extraction with 50 mM ammonium bicarbonate and 100% acetonitrile. The resulting peptide extracts for each band were lyophilized and stored at -20  $^{\circ}$ C until mass spectrometric analysis.

### LC-MS/MS protein analysis

Peptides were analyzed using a nanoflow LC-MS/MS system consisting of an Easy nLC 1000 system (Thermo Fisher) and an LTQ Orbitrap Elite mass spectrometer (Thermo Fisher) equipped with a nano-electrospray source. Peptide solutions (5- $\mu$ l aliquots) were loaded onto a C<sub>18</sub> trap column (20  $\times$  75  $\mu$ m, 3  $\mu$ m particle size; Thermo Fisher) using an autosampler. Peptides were desalted and concentrated on the column at a flow rate of 5  $\mu$ l/min. Trapped peptides were then separated on a 150-mm custom-built microcapillary column consisting of C<sub>18</sub> (particle size, 3  $\mu$ m; Aqua Science, Yokohama, Japan) packed in 100- $\mu$ m silica tubing with a 6- $\mu$ m inner diameter orifice. The mobile phases A and B were composed of 0 and 100% acetonitrile, respectively, and each contained 0.1% formic acid. The LC gradient began with 5% B for 5 min and was increased to 15% B over 5 min, 50% B over 55 min, and 95% B over 5 min, then remained at 95% B over 5 min, followed by 5% B for an additional 5 min. The column was re-equilibrated with 5% B for 15 min between runs. A voltage of 2.2 kV was applied to produce the electrospray. In each mass analysis duty cycle, one high-mass resolution (60,000) MS spectrum was acquired using the Orbitrap analyzer, followed by 10 data-dependent MS/MS scans using the linear ion trap analyzer. For MS/MS analysis, a normalized collision energy (35%) was used throughout the collision-induced dissociation phase. All MS and MS/MS spectra were acquired using the following parameters: no sheath and

auxiliary gas flow; ion-transfer tube temperature, 200 °C; activation Q, 0.25; and activation time, 20 ms. Dynamic exclusion was employed with a repeat count of 1, a repeat duration of 30 s, an exclusion list size of 500, an exclusion duration of 60 s, and an exclusion mass width of  $\pm 1.5$  m/z.

### MS data analysis

MS/MS spectra were analyzed using the following analysis protocol, referencing the UniProt mouse database (04-08-2020 release; 17,333 entries). Briefly, each protein's reversed sequence was appended onto the database to calculate the false discovery rate. Peptides were identified using ProLuCID (version 1.3.5.1) (40) in Integrated Proteomics Pipeline software, IP2, with a precursor mass error of 25 ppm and a fragment ion mass error of 600 ppm. Trypsin was used as the protease, and two potential missed cleavages were allowed. Carbamidomethylation at cysteine was chosen as a static modification, and methionine oxidation was chosen as a variable modification. Protein lists consisting of two or more peptide assignments for protein identification (false-positive rate <0.01) were prepared by filtering and sorting output data files.

### Primary neuron culture, immunocytochemistry, image acquisition, and quantitative analysis

The indicated analyses were performed using cultured, E18-derived, rat hippocampal neurons and confocal microscopy, as previously described (15, 41, 42). Rat hippocampal neurons were prepared from E18 rat brains and cultured on coverslips coated with poly-D-lysine in Neurobasal media supplemented with B-27 (Thermo Fisher), 0.5% fetal bovine serum, 0.5 mM GlutaMax (Thermo Fisher), and sodium pyruvate (Thermo Fisher). For immunocytochemistry, cultured neurons were fixed with 4% formaldehyde, 4% sucrose, permeabilized with 0.2% Triton X-100 in PBS, and immunostained with primary antibodies and Cy3- or FITC-conjugated secondary antibodies (Jackson ImmunoResearch, West Grove, PA, USA). Images were acquired using a confocal microscope (LSM700; Carl Zeiss) equipped with a 63 $\times$  objective lens. All image settings were kept constant. Z-stack images were converted to maximal projection. All images were quantitatively analyzed in a blinded manner using MetaMorph software (Molecular Devices).

### Cell surface-binding assays

Ig-fusion proteins of *Clstn3*, *IgNrxn1 $\beta$*  splice variants, and IgC alone (Control) were produced in HEK293T cells. Soluble Ig-fused proteins were purified using protein A-Sepharose beads (GE Healthcare). Bound proteins were eluted with 0.1 M glycine (pH 2.5) and immediately neutralized with 1 M Tris-HCl (pH 8.0). Transfected HEK293T cells expressing the indicated plasmids were incubated with 10  $\mu$ g/ml of Ig-fused proteins for 2 h at 37 °C. Images were acquired using a confocal microscope (LSM700; Carl Zeiss).

### Pulldown assays

HEK293T cells were transfected with pGW1-FLAG-*Clstn3* Full, Cad,  $\Delta$ Cad, or pCMV-mVenus-NL-1, harvested 48 h later,

and incubated for 1 h at 4 °C in solubilization buffer (25 mM Tris-HCl, pH 7.6, 150 mM NaCl, 1% octylphenoxypolyethoxyethanol, 1% sodium deoxycholate, 0.1% SDS, 5 mM CaCl<sub>2</sub>, 5 mM MgCl<sub>2</sub>). The suspension was centrifuged at 20,000  $\times$  g to remove insoluble debris, and each supernatant was mixed with 10  $\mu$ g of IgC (control), *IgNrxn1 $\alpha$ <sup>+SS4</sup>*, or *IgNrxn1 $\beta$ <sup>+SS4</sup>* supplemented with protein A-Sepharose beads and incubated at 4 °C for 2 h with gentle agitation. For *in vivo* pulldown assays, synaptosomal fractions prepared from mouse brains were mixed with 10  $\mu$ g of IgC (control), *IgNrxn1 $\alpha$ <sup>-SS4</sup>*, *IgNrxn1 $\alpha$ <sup>+SS4</sup>*, *IgNrxn1 $\beta$ <sup>-SS4</sup>*, or *IgNrxn1 $\beta$ <sup>+SS4</sup>* and incubated at 4 °C for 2 h with gentle agitation. Protein A-Sepharose beads were washed three times with solubilization buffer, solubilized in SDS sample buffer, and loaded onto SDS-PAGE gels for immunoblot analyses. The antibodies used for immunoblotting were anti-FLAG (1  $\mu$ g/ml), anti-EGFP (1:1000), anti-*Clstn3* (JK091; 1  $\mu$ g/ml), anti-NL-1 (1  $\mu$ g/ml), anti-NL-2 (1  $\mu$ g/ml), and anti-TrkC (1  $\mu$ g/ml).

### Direct protein-interaction assays

For direct interaction assays, 10  $\mu$ g of IgC (control), *IgNrxn1 $\alpha$ <sup>-SS4</sup>*, *IgNrxn1 $\alpha$ <sup>+SS4</sup>*, *IgNrxn1 $\beta$ <sup>-SS4</sup>*, or *IgNrxn1 $\beta$ <sup>+SS4</sup>* was incubated with 4  $\mu$ g of purified His-HA-*Clstn3* Full, His-HA-*Clstn3* Cad, or His-HA-*Clstn3*  $\Delta$ Cad for 2 h at 4 °C in binding buffer (25 mM Tris, pH 7.5, 30 mM MgCl<sub>2</sub>, 40 mM NaCl, and 0.5% Triton X-100). Talon metal affinity resins (Clontech) beads were then added to purified protein mixtures as indicated, and incubated for 2 h at 4 °C. Beads were washed three times with binding buffer, solubilized in SDS sample buffer, and loaded onto SDS-PAGE gels for immunoblot analyses. Anti-human IgG was used for immunoblotting.

### Heterologous synapse-formation assays

Heterologous synapse-formation assays were performed using recombinant *Clstn3* fusion proteins as previously described (43). Briefly, HEK293T cells were transfected with EGFP (negative control) or the indicated *Clstn3* constructs using Lipofectamine 2000 (Thermo Fisher). After 48 h, the transfected HEK293T cells were trypsinized, seeded onto *in vitro* day 10 (DIV10) hippocampal neurons, co-cultured for an additional 72 h, and double-immunostained on DIV13 with antibodies against EGFP, HA, and the indicated synaptic markers (synapsin, VGLUT1, or GAD67). All images were acquired using a confocal microscope (LSM700; Zeiss). For quantification, the contours of transfected HEK293T cells were chosen as the region of interest. Fluorescence intensities of synaptic markers in each region of interest were quantified for both red and green channels using MetaMorph software (Molecular Devices). Normalized synapse density on transfected HEK293T cells was expressed as the ratio of red to green fluorescence.

### Semiquantitative immunoblot analysis

For semiquantitative immunoblot analysis, brains from P42 WT, *Clstn3<sup>fl/fl</sup>*, or *Clstn3<sup>fl/fl</sup>::Nestin-Cre* (*Nestin-Clstn3*) mice were homogenized in 0.32 M sucrose, 1 mM MgCl<sub>2</sub> containing a protease inhibitor mixture (Thermo Fisher Scientific) using a

## Interaction of *Clstn3* with $\alpha/\beta$ -Nrxns

Precellys Evolution tissue homogenizer (Bertin Co.). After centrifuging homogenates at  $1,000 \times g$  for 10 min, the supernatant was transferred to a fresh microcentrifuge tube and centrifuged at  $15,000 \times g$  for 30 min. The resulting synaptosome-enriched pellet (P2) was resuspended in lysis buffer and centrifuged at  $20,800 \times g$ , after which the supernatant was analyzed by Western blotting. Quantitation was performed using ImageJ software (National Institutes of Health).

### Immunohistochemistry

Mice were transcardially perfused first with PBS and then with 4% paraformaldehyde. After post-fixation overnight, mouse brains were slowly sectioned at  $40 \mu\text{M}$  using a vibratome (VT1200S; Leica) and washed with PBS. Brain sections were incubated in blocking solution containing 10% horse serum, 0.2% BSA, and 2% Triton X-100 for 1 h at room temperature, and then incubated overnight at  $4^\circ\text{C}$  with primary antibodies against VGLUT1 (1:200), GAD67 (1:100), GAD65 (1:300), GABA<sub>A</sub>R $\gamma$ 2 (1:500), PSD-95 (1:100), *Clstn3* (JK091; 1:100), or NeuN (1:500). After washing three times, sections were incubated with Cy3- or FITC-conjugated secondary antibodies (Jackson ImmunoResearch, West Grove, PA, USA) for 2 h at room temperature. Sections were then washed extensively, and mounted on glass slides with Vectashield Mounting Medium (Vector Laboratories). Images were acquired by slide scanner microscopy (AxioScan.Z1; Zeiss).

### Nissl staining

Mice were perfused first with PBS and then with 4% paraformaldehyde by cardiac injection. Fixed brain tissue was isolated, post-fixed for 12 h at  $4^\circ\text{C}$ , and dehydrated in 30% sucrose for 1–2 days. Thereafter, brain tissue was embedded in OCT (optimal cutting temperature) compound and stored at  $-80^\circ\text{C}$ . The frozen tissue was mounted and cut at a thickness of  $20 \mu\text{m}$  using a cryostat (Leica CM5120). Slices were mounted on glass slides, washed three times with PBS (15 min each), and permeabilized with 0.1% Triton X-100 in PBS for 10 min. Permeabilized slices were washed twice with PBS (5 min each), then incubated for 20 min in  $200 \mu\text{l}$  of NeuroTrace 500/525 Green Fluorescent Nissl Stain (Molecular Probes), diluted 1:100 in PBS before use. Thereafter slices were washed in PBS containing 0.1% Triton X-100 for 10 min, then washed twice in PBS (5 min each) and incubated in PBS for 2 h. Slides were dried and mounted using Vectashield mounting medium containing 4',6-diamidino-2-phenylindole (DAPI; Vector Laboratories). Green fluorescence was imaged by slide scanner microscopy (AxioScan.Z1; Zeiss).

### Fluorescent *in situ* hybridization (RNAscope assay)

Frozen sections ( $14 \mu\text{m}$  thick) were cut coronally through the hippocampal formation and thaw-mounted onto Superfrost Plus microscope slides (Advanced Cell Diagnostics). Sections were fixed in 4% formaldehyde for 10 min, dehydrated in increasing concentrations of ethanol for 5 min, air dried, and then pretreated with protease for 10 min at room temperature. For RNA detection, sections were incubated in different amplifier solutions in a HybEZ hybridization oven (Advanced Cell

Diagnostics) at  $40^\circ\text{C}$ . Three synthetic oligonucleotides complementary to the sequence corresponding to nucleotide residues 302–1210 of Mm-*Clstn3*-tv1, 896–1986 of Mm-CaMKII $\alpha$ -C2, 18–407 of Mm-SST-C3, and 2–885 of Mm-Pvalb-C3 (Advanced Cell Diagnostics) were used as probes. The labeled probes were conjugated to Alexa Fluor 488, Alto 550, or Alto 647, after which labeled probe mixtures were hybridized by incubating with slide-mounted sections for 2 h at  $40^\circ\text{C}$ . Non-specifically hybridized probes were removed by washing the sections three times for 2 min each with  $1\times$  wash buffer at room temperature, followed by incubation with Amplifier 1-FL for 30 min, Amplifier 2-FL for 15 min, Amplifier 3-FL for 30 min, and Amplifier 4 Alt B-FL for 15 min at  $40^\circ\text{C}$ . Each amplifier was removed by washing with  $1\times$  wash buffer for 2 min at room temperature. Slides were imaged with an LSM700 microscope (Zeiss) and analyzed using MetaMorph software (Molecular Devices).

### Stereotaxic injection of rAAVs

Adult ( $\sim 9$ -week-old) male mice were anesthetized with Avertin (400 mg/kg body weight) by intraperitoneal injection. rAAV solutions (titers  $\geq 1 \times 10^{11}$  viral genomes/ml) were injected with a NanoFil syringe (World Precision Instruments) at a flow rate of  $0.1 \mu\text{l}/\text{min}$ . The coordinates used for the CA1 region of the dorsal hippocampus were AP  $-2.5 \text{ mm}$ , ML  $\pm 1.5 \text{ mm}$ , DV  $+1.5 \text{ mm}$  (from the dura). The site at DV  $+1.5 \text{ mm}$  received a  $1\text{-}\mu\text{l}$  injection. Injected mice were allowed to recover for at least 14 days following surgery prior to use in experiments.

### Electrophysiology

Electrophysiological recordings were performed in acute hippocampal CA1 slices. Mice were anesthetized with isoflurane and decapitated. Their brains were rapidly removed and placed in ice-cold, oxygenated (95% O<sub>2</sub> and 5% CO<sub>2</sub>) low Ca<sup>2+</sup>/high Mg<sup>2+</sup> solution containing the following: 3.3 mM KCl, 1.3 mM NaH<sub>2</sub>PO<sub>4</sub>, 26 mM NaHCO<sub>3</sub>, 11 mM D-glucose, 0.5 mM CaCl<sub>2</sub>, 10 mM MgCl<sub>2</sub>, and 211 mM sucrose. Slices were equilibrated at  $30^\circ\text{C}$  for at least 60 min in oxygenated artificial cerebrospinal fluid, consisting of the following: 124 mM NaCl, 3.3 mM KCl, 1.3 mM NaH<sub>2</sub>PO<sub>4</sub>, 26 mM NaHCO<sub>3</sub>, 11 mM D-glucose, 3.125 mM CaCl<sub>2</sub>, and 2.25 mM MgCl<sub>2</sub>. Slices were then transferred to a recording chamber, where they were maintained at  $24\text{--}27^\circ\text{C}$  and perfused continuously with 95% O<sub>2</sub>- and 5% CO<sub>2</sub>-bubbled artificial cerebrospinal fluid. Whole cell recordings of miniature postsynaptic currents were performed on CA1 pyramidal neurons voltage clamped at  $-70 \text{ mV}$ . Glass pipettes were filled with an internal solution containing the following: 130 mM CsMeSO<sub>4</sub>, 0.5 mM EGTA, 5 mM tetraethylammonium-Cl, 8 mM NaCl, 10 mM HEPES, 1 mM QX-314, 4 mM Mg-ATP, 0.4 mM Na-GTP, and 10 mM phosphocreatine-Na<sub>2</sub> for mEPSCs; 130 mM CsCl, 1.1 mM EGTA, 2 mM MgCl<sub>2</sub>, 0.1 mM CaCl<sub>2</sub>, 10 mM NaCl, 10 mM HEPES, and 2 mM Na-ATP for mIPSCs. The osmolarity of the internal solution was 290–300 mOsm (pH 7.3; adjusted with CsOH). For mEPSC recordings,  $1 \mu\text{M}$  TTX,  $50 \mu\text{M}$  DL-2-amino-5-phosphonopentanoic acid, and  $100 \mu\text{M}$  picrotoxin were added to block Na<sup>+</sup> currents, NMDA receptors, and GABA<sub>A</sub> receptors, respectively. For mIPSC

recordings, 1  $\mu\text{M}$  TTX, 20  $\mu\text{M}$  6-cyano-7-nitroquinoxaline-2,3-dione, 50  $\mu\text{M}$  DL-2-amino-5-phosphonopentanoic acid were added to block  $\text{Na}^+$  currents,  $\alpha$ -amino-3-hydroxy-5-methyl-4-isoxazolepropionic acid and NMDA receptors, respectively.

### Statistical analysis

All data are expressed as mean  $\pm$  S.E., and significance is indicated with asterisk (compared with a value from control group) or hashtag (compared with a value from experimental group). *N* values are denoted in the individual figure legends. For cell surface-binding and heterologous synapse-formation assays, cells used for analysis were obtained from 5 to 10 images from at least three independent experiments. The normality of data distributions was evaluated using the Shapiro-Wilk test, followed by nonparametric Kruskal-Wallis test with Dunn's multiple comparison test for post hoc group comparisons or ANOVA with Tukey's test, using cell numbers or the number of experiments as the basis for *n*.

### Data availability

All data except MS data are contained within this article and the [supporting information](#). All raw MS and supporting data files from the current study have been deposited to the repository of MassIVE with identifier [PXD018433](#).

**Author contributions**—J. Ko and J. W. U. conceptualization; H. Kim, D. K., J. Kim, and H-Y. L. data curation; H. Kim, D. K., J. Kim, H-Y. L., D. P., J. Y. K., S-Y. C., J. Ko, and J. W. U. formal analysis; S. -Y. C., J. Ko, and J. W. U. supervision; J. Y. K., J. Ko, and J. W. U. funding acquisition; H. Kim, D. K., and J. Kim validation; H. Kim, D. K., J. Kim, H-Y. L., D. P., H. Kang, K.M., S-Y. C., J. Ko, and J. W. U. investigation; H. Kim, D. K., J. Kim, H-Y. L., D. P., H. Kang, K. M., and J. W. U. methodology; J. Ko and J. W. U. writing-original draft; J. Ko and J. W. U. project administration; H. Kim, J. Ko, and J. W. U. writing-review and editing; K. M., F. H. S., M. Y., and J. Y. K. resources.

**Funding and additional information**—This work was supported by National Research Foundation of Korea (NRF), Ministry of Science and ICT Grants 2019R1A2C1086048 (to J. W. U.), 2019R1A2B5B02069324 (to J. Ko), and 2017M3C7A1023470 (to J. Ko), KBSI Grant C060100 (to J. Y. K.).

**Conflict of interest**—The authors declare that they have no conflicts of interest with the contents of this article.

**Abbreviations**—The abbreviations used are: Nrxn, neurexin; AAV, adeno-associated virus; Cad, cadherin; *Clstn3*, calyntenin-3; GAD65, glutamic acid decarboxylase 65; GAD67, glutamic acid decarboxylase 67; LAR-RPTPs, leukocyte common antigen-related receptor protein-tyrosine phosphatases; LNS, laminin, neurexin, sex-hormone binding globulin; LTP, long-term potentiation; LRRTM, leucine-rich repeat transmembrane neuronal protein; NL, neuroligin; NMDA, *N*-methyl-d-aspartate; SLM, stratum lacunosum moleculare; SO, stratum oriens; SP, stratum pyramidale; SR, stratum radiatum; SS4, splice site 4; TKD, triple-knockdown; VGLUT1, vesicular glutamate transporter 1; PV, parvalbumin; SST, somatostatin; mIPSC, miniature inhibitory postsynaptic current; mEPSC,

miniature excitatory postsynaptic currents; aa, amino acid(s); HA, hemagglutinin; DAPI, 4[prime],6-diamidino-2-phenylindole; EGFP, enhanced green fluorescent protein; TTX, tetrodotoxin; P30, post-natal day 30; ANOVA, analysis of variance.

### References

- Missler, M., Südhof, T. C., and Biederer, T. (2012) Synaptic cell adhesion. *Cold Spring Harb. Perspect. Biol.* **4**, a005694 [CrossRef Medline](#)
- Um, J. W., and Ko, J. (2013) LAR-RPTPs: synaptic adhesion molecules that shape synapse development. *Trends Cell Biol.* **23**, 465–475 [CrossRef Medline](#)
- Südhof, T. C. (2017) Synaptic neurexin complexes: a molecular code for the logic of neural circuits. *Cell* **171**, 745–769 [CrossRef Medline](#)
- Ko, J., Choi, G., and Um, J. W. (2015) The balancing act of GABAergic synapse organizers. *Trends Mol. Med.* **21**, 256–268 [CrossRef Medline](#)
- Südhof, T. C. (2018) Towards an understanding of synapse formation. *Neuron* **100**, 276–293 [CrossRef Medline](#)
- Han, K. A., Jeon, S., Um, J. W., and Ko, J. (2016) Emergent synapse organizers: LAR-RPTPs and their companions. *Int. Rev. Cell Mol. Biol.* **324**, 39–65 [CrossRef Medline](#)
- Sotomayor, M., Gaudet, R., and Corey, D. P. (2014) Sorting out a promiscuous superfamily: towards cadherin connectomics. *Trends Cell Biol.* **24**, 524–536 [CrossRef Medline](#)
- Ster, J., Steuble, M., Orlando, C., Diep, T. M., Akhmedov, A., Raineteau, O., Pernet, V., Sonderegger, P., and Gerber, U. (2014) Calyntenin-1 regulates targeting of dendritic NMDA receptors and dendritic spine maturation in CA1 hippocampal pyramidal cells during postnatal development. *J. Neurosci.* **34**, 8716–8727 [CrossRef Medline](#)
- Alther, T. A., Domanitskaya, E., and Stoeckli, E. T. (2016) Calyntenin 1-mediated trafficking of axon guidance receptors regulates the switch in axonal responsiveness at a choice point. *Development* **143**, 994–1004 [CrossRef Medline](#)
- Ponomareva, O. Y., Holmen, I. C., Sperry, A. J., Eliceiri, K. W., and Halloran, M. C. (2014) Calyntenin-1 regulates axon branching and endosomal trafficking during sensory neuron development *in vivo*. *J. Neurosci.* **34**, 9235–9248 [CrossRef Medline](#)
- Lee, T. J., Lee, J. W., Haynes, E. M., Eliceiri, K. W., and Halloran, M. C. (2017) The kinesin adaptor calyntenin-1 organizes microtubule polarity and regulates dynamics during sensory axon arbor development. *Front. Cell Neurosci.* **11**, 107 [CrossRef Medline](#)
- Lipina, T. V., Prasad, T., Yokomaku, D., Luo, L., Connor, S. A., Kawabe, H., Wang, Y. T., Brose, N., Roder, J. C., and Craig, A. M. (2016) Cognitive deficits in calyntenin-2-deficient mice associated with reduced GABAergic transmission. *Neuropsychopharmacology* **41**, 802–810 [CrossRef Medline](#)
- Ranneva, S. V., Pavlov, K. S., Gromova, A. V., Amstislavskaya, T. G., and Lipina, T. V. (2017) Features of emotional and social behavioral phenotypes of calyntenin2 knockout mice. *Behav. Brain Res.* **332**, 343–354 [CrossRef Medline](#)
- Pettem, K. L., Yokomaku, D., Luo, L., Linhoff, M. W., Prasad, T., Connor, S. A., Siddiqui, T. J., Kawabe, H., Chen, F., Zhang, L., Rudenko, G., Wang, Y. T., Brose, N., and Craig, A. M. (2013) The specific  $\alpha$ -neurexin interactor calyntenin-3 promotes excitatory and inhibitory synapse development. *Neuron* **80**, 113–128 [CrossRef Medline](#)
- Um, J. W., Pramanik, G., Ko, J. S., Song, M. Y., Lee, D., Kim, H., Park, K. S., Südhof, T. C., Tabuchi, K., and Ko, J. (2014) Calyntenins function as synaptogenic adhesion molecules in concert with neurexins. *Cell Rep.* **6**, 1096–1109 [CrossRef Medline](#)
- Ko, J., Fuccillo, M. V., Malenka, R. C., and Südhof, T. C. (2009) LRRTM2 functions as a neurexin ligand in promoting excitatory synapse formation. *Neuron* **64**, 791–798 [CrossRef Medline](#)
- Missler, M., Hammer, R. E., and Südhof, T. C. (1998) Neurexophilin binding to  $\alpha$ -neurexins: a single LNS domain functions as an independently folding ligand-binding unit. *J. Biol. Chem.* **273**, 34716–34723 [CrossRef Medline](#)

## Interaction of *Clstn3* with $\alpha/\beta$ -*Nrxns*

18. Boucard, A. A., Ko, J., and Südhof, T. C. (2012) High affinity neurexin binding to cell adhesion G-protein-coupled receptor C1RL1/latrophilin-1 produces an intercellular adhesion complex. *J. Biol. Chem.* **287**, 9399–9413 [CrossRef Medline](#)
19. Sterky, F. H., Trotter, J. H., Lee, S. J., Recktenwald, C. V., Du, X., Zhou, B., Zhou, P., Schwenk, J., Fakler, B., and Südhof, T. C. (2017) Carbonic anhydrase-related protein CA10 is an evolutionarily conserved pan-neurexin ligand. *Proc. Natl. Acad. Sci. U.S.A.* **114**, E1253–E1262 [CrossRef Medline](#)
20. Um, J. W., Choi, T. Y., Kang, H., Cho, Y. S., Choi, G., Uvarov, P., Park, D., Jeong, D., Jeon, S., Lee, D., Kim, H., Lee, S. H., Bae, Y. C., Choi, S. Y., Airaksinen, M. S., et al. (2016) LRRTM3 regulates excitatory synapse development through alternative splicing and neurexin binding. *Cell Rep.* **14**, 808–822 [CrossRef Medline](#)
21. Skarnes, W. C., Rosen, B., West, A. P., Koutsourakis, M., Bushell, W., Iyer, V., Mujica, A. O., Thomas, M., Harrow, J., Cox, T., Jackson, D., Severin, J., Biggs, P., Fu, J., Nefedov, M., et al. (2011) A conditional knockout resource for the genome-wide study of mouse gene function. *Nature* **474**, 337–342 [CrossRef Medline](#)
22. Reissner, C., Runkel, F., and Missler, M. (2013) Neurexins. *Genome Biol.* **14**, 213 [CrossRef Medline](#)
23. Lu, Z., Wang, Y., Chen, F., Tong, H., Reddy, M. V., Luo, L., Seshadrinathan, S., Zhang, L., Holthausen, L. M., Craig, A. M., Ren, G., and Rudenko, G. (2014) Calsyntenin-3 molecular architecture and interaction with neurexin 1 $\alpha$ . *J. Biol. Chem.* **289**, 34530–34542 [CrossRef Medline](#)
24. Kim, B., and Emmons, S. W. (2017) Multiple conserved cell adhesion protein interactions mediate neural wiring of a sensory circuit in *C. elegans*. *Elife* **6**, e29257 [CrossRef](#)
25. Colavita, A., and Tessier-Lavigne, M. (2003) A neurexin-related protein, BAM-2, terminates axonal branches in *C. elegans*. *Science* **302**, 293–296 [CrossRef Medline](#)
26. Iijima, T., Wu, K., Witte, H., Hanno-Iijima, Y., Glatter, T., Richard, S., and Scheiffele, P. (2011) SAM68 regulates neuronal activity-dependent alternative splicing of neurexin-1. *Cell* **147**, 1601–1614 [CrossRef Medline](#)
27. Dai, J., Aoto, J., and Südhof, T. C. (2019) Alternative splicing of presynaptic neurexins differentially controls postsynaptic NMDA and AMPA receptor responses. *Neuron* **102**, 993–1008.e5 [CrossRef](#)
28. Basu, R., Duan, X., Taylor, M. R., Martin, E. A., Muralidhar, S., Wang, Y., Gangi-Wellman, L., Das, S. C., Yamagata, M., West, P. J., Sanes, J. R., and Williams, M. E. (2017) Heterophilic type II cadherins are required for high-magnitude synaptic potentiation in the hippocampus. *Neuron* **96**, 160–176.e168 [CrossRef Medline](#)
29. Ullrich, B., Ushkaryov, Y. A., and Südhof, T. C. (1995) Cartography of neurexins: more than 1000 isoforms generated by alternative splicing and expressed in distinct subsets of neurons. *Neuron* **14**, 497–507 [CrossRef Medline](#)
30. Nguyen, T. M., Schreiner, D., Xiao, L., Traummüller, L., Bornmann, C., and Scheiffele, P. (2016) An alternative splicing switch shapes neurexin repertoires in principal neurons versus interneurons in the mouse hippocampus. *Elife* **5**, e22757 [CrossRef](#)
31. Uchigashima, M., Cheung, A., Suh, J., Watanabe, M., and Futai, K. (2019) Differential expression of neurexin genes in the mouse brain. *J. Comp. Neurol.* **527**, 1940–1965 [CrossRef](#)
32. Ikeda, D. D., Duan, Y., Matsuki, M., Kunitomo, H., Hutter, H., Hedgecock, E. M., and Iino, Y. (2008) CASY-1, an ortholog of calyntenins/alcadeins, is essential for learning in *Caenorhabditis elegans*. *Proc. Natl. Acad. Sci. U.S.A.* **105**, 5260–5265 [CrossRef Medline](#)
33. Thapliyal, S., Vasudevan, A., Dong, Y., Bai, J., Koushika, S. P., and Babu, K. (2018) The C-terminal of CASY-1/Calsyntenin regulates GABAergic synaptic transmission at the *Caenorhabditis elegans* neuromuscular junction. *PLoS Genet.* **14**, e1007263 [CrossRef Medline](#)
34. Lee, K., Kim, Y., Lee, S. J., Qiang, Y., Lee, D., Lee, H. W., Kim, H., Je, H. S., Südhof, T. C., and Ko, J. (2013) MDGAs interact selectively with neuroligin-2 but not other neuroligins to regulate inhibitory synapse development. *Proc. Natl. Acad. Sci. U.S.A.* **110**, 336–341 [CrossRef Medline](#)
35. Ko, J., Soler-Llavina, G. J., Fuccillo, M. V., Malenka, R. C., and Südhof, T. C. (2011) Neuroligins/LRRTMs prevent activity- and Ca<sup>2+</sup>/calmodulin-dependent synapse elimination in cultured neurons. *J. Cell Biol.* **194**, 323–334 [CrossRef Medline](#)
36. Matsuda, K., and Yuzaki, M. (2011) Cbln family proteins promote synapse formation by regulating distinct neurexin signaling pathways in various brain regions. *Eur. J. Neurosci.* **33**, 1447–1461 [CrossRef Medline](#)
37. Han, K. A., Woo, D., Kim, S., Choi, G., Jeon, S., Won, S. Y., Kim, H. M., Heo, W. D., Um, J. W., and Ko, J. (2016) Neurotrophin-3 regulates synapse development by modulating TrkC-PTP $\sigma$  synaptic adhesion and intracellular signaling pathways. *J. Neurosci.* **36**, 4816–4831 [CrossRef Medline](#)
38. Han, K. A., Kim, J., Kim, H., Kim, D., Lim, D., Ko, J., and Um, J. W. (2019) Slitrk2 controls excitatory synapse development via PDZ-mediated protein interactions. *Sci. Rep.* **9**, 17094 [CrossRef Medline](#)
39. Kim, M. H., Choi, J., Yang, J., Chung, W., Kim, J. H., Paik, S. K., Kim, K., Han, S., Won, H., Bae, Y. S., Cho, S. H., Seo, J., Bae, Y. C., Choi, S. Y., and Kim, E. (2009) Enhanced NMDA receptor-mediated synaptic transmission, enhanced long-term potentiation, and impaired learning and memory in mice lacking IRSp53. *J. Neurosci.* **29**, 1586–1595 [CrossRef Medline](#)
40. Xu, T., Park, S. K., Venable, J. D., Wohlschlegel, J. A., Diedrich, J. K., Cociorva, D., Lu, B., Liao, L., Hewel, J., Han, X., Wong, C. C., Fonslow, B., Delahunty, C., Gao, Y., Shah, H., et al. (2015) ProLuCID: An improved SEQUEST-like algorithm with enhanced sensitivity and specificity. *J. Proteomics* **129**, 16–24, 3rd [CrossRef Medline](#)
41. Um, J. W., Kim, K. H., Park, B. S., Choi, Y., Kim, D., Kim, C. Y., Kim, S. J., Kim, M., Ko, J. S., Lee, S. G., Choi, G., Nam, J., Heo, W. D., Kim, E., Lee, J. O., et al. (2014) Structural basis for LAR-RPTP/Slitrk complex-mediated synaptic adhesion. *Nat. Commun.* **5**, 5423 [CrossRef Medline](#)
42. Kang, H., Han, K. A., Won, S. Y., Kim, H. M., Lee, Y. H., Ko, J., and Um, J. W. (2016) Slitrk missense mutations associated with neuropsychiatric disorders distinctively impair Slitrk trafficking and synapse formation. *Front. Mol. Neurosci.* **9**, 104 [CrossRef Medline](#)
43. Ko, J., Zhang, C., Arac, D., Boucard, A. A., Brunger, A. T., and Südhof, T. C. (2009) Neuroligin-1 performs neurexin-dependent and neurexin-independent functions in synapse validation. *EMBO J.* **28**, 3244–3255 [CrossRef Medline](#)